Physics
Cole Memorial Library

SCIENCE OF LIGHT

VOLUME 5 NUMBER 3

December

1956

OHIO STATE UNIVERSITY
MAR 11 1958
LIBRARY

Published by the

Institute for Optical Research

Tokyo University of Education

in collaboration with the

The Spectroscopical Society of Japan

SCIENCE OF LIGHT

Science of Light contains reports of the Institute for Optical Research and contributions from other science bodies about similar subjects.

The editorial staff consists of following members:

Chairman: Prof. H. Ootsuka, *Tokyo University of Education*

Dr. Y. Fujioka, *Atomic Energy Commission of Japan*

Prof. E. Minami, *Tokyo University*

Prof. M. Seya, *Tokyo University of Education*

Prof. Y. Uchida, *Kyoto University*

Prof. T. Uemura, *Rikkyo University*

Prof. K. Miyake, *Tokyo University of Education*

All communications should be addressed to the director or to the librarian of the Institute.

The Institute for Optical Research

Tokyo University of Education

400, 4-chome, Hyakunin-machi, Sinjuku-ku, Tokyo, Japan

Printed at
Kokusai Bunken Insatsusha
Chiyoda-ku, Tokyo.

Double Beam Infrared Spectrophotometer Using Double Pass, Triple Pass, Double Monochromator and Double Pass Double Monochromator

Keiei KUDO

Institute for Optical Research, Tokyo University of Education

(Received September 15, 1956)

Abstract

Double beam double or triple pass infrared spectrophotometer using Lochester and Martin's method and double beam double monochro infrared spectrophotometer in which each monochromator is of single pass or fore monochromator is of single pass and rear monochromator is of double pass using Walsh's method have been constructed, and the increase of resolution, the scanning speed and the effect of false radiation are examined and discussed.

These spectrophotometers have higher resolution and faster scanning speed than a common single pass instrument. But as far as the effect of false radiation is concerned, multiple pass spectrophotometer using double monochromator exceeds to that using Lochester and Martin's method.

1. Introduction

Single beam double or multiple pass infrared spectophotometer invented by Walsh[1] shows higher resolution than a single pass infrared spectrophotometer. However, with such a single beam type, spectrum is strongly disturbed by atmospheric absorption lines unless it is operated in vaccum. Therefore, spectral analysis using such a single beam type is very tedious.

With a double beam type, the atmospheric lines have no effect, and at the same time percent transmission or optical density of samples is directly obtained. However, almost all double beam instruments[2] published up to the present are of single pass, and the author[3] also reported about one of these types.

An infrared spectrophotometer with a higher resolution, faster scanning speed and smaller effect of false radiation than a single pass instrument will be

1) A. Walsh: Nature **167** (1951) 870.
N. S. Ham, A. Walsh and J. B. Wills: J. Opt. Soc. Amer. **42** (1952) 496.
2) For example,
W. S. Baird, H. M. O'Bryan, G. Ogden and D. Lee: J. Opt. Soc. Amer. **37** (1947) 754.
J. D. White and M. D. Liston: J. Opt. Soc. Amer. **40** (1950) 29.
3) K. Kudo: Science of Light **4** (1955) 85.

more advantageous to spectrochemical analysts.

In order to obtain a high resolution, a method to increase angular dispersion of a prism must be devised by all means. To increase the scanning speed, it is necessary to obtain intensive optical signal, and to decrease or eliminate the effect of false radiation, arrangement of monochromator must be considered.

Bechman IR-4[4], which is a common double monochromator, is an example that solved these problems to some extent. There has been no systematic comparative study on various types of infrared spectrophotometer by turning them out by way of experimentation. The purpose of the present work is to examine methodically the resolution, scanning speed and the effect of false radiation of various double beam infrared spectrophotometers (some with double monochromator) in which the prism is used doubly or multiply.

2. Theoretical Consideration

(*a*) *Resolution*

If the aberration of the optical system is negligible, resolution of infrared spectrophotometer is determined by the resolving power of the prism and the spectral slit width which is, in its turn, determined by the focal length of the collimator and the angular dispersion of the prism. Let us consider the resolutions of spectra of one and the same sample recorded under the condition of a given signal-to-noise ratio by a single pass ($n=1$) and a double or multiple pass ($n \geq 2$) spectrophotometer, the latter with or without a double monochronomator and both with supposedly identical parts except the prism.

Available energy $I_n(\lambda)$ through the monochromator is proportional to the square of slit width W_n^2, transmittance of prism material $T_n(\lambda)$ and the transmission through surfaces $F_n(\lambda)$ and inversely proportional to the angular dispersion of prism $D_n(\lambda)$.

If the light traverses the prism n times,

$$I_n \sim W_n^2 T_n F_n / D_n \qquad (1)$$

where $D_n = nD_1$.

By chopping this available energy, the detector produces a.c. signals. The signal is amplified, rectified and finally fed to the control motor, and so is also the Johnson noise in the detector. If these spectrophotometers have detectors of the same characteristics, the electromotive force of the noise in detectors will be definite, and to have the same signal-to-noise ratio for the spectrophotometers,

4) Bechman infrared notes. Vol. **2**. No. 1.

I_n should be equal to I_1. Hence from Expression (1).

$$W_n/W_1=(nT_1F_1/T_nF_n)^{1/2} \qquad (2)$$

It will be seen that the ratio of the slit widths W_n/W_1 is larger than $\sqrt{n}$ since $T_1F_1/T_nF_n)>1$ in the case of $n\lesssim 2$. In order to simplify calculation, let us consider the minimum deviation type. Since the prism in Littrow type is fixed at minimum deviation at a certain wavelength λ, calculation for the minimum deviation type at a wavelength near λ is approximately correct for the Littrow type. In such a case, $T_n(\lambda)$ is easily obtained from Strong's table[5], and as for $F_n(\lambda)$, Fernell's expression is used. Now taking a NaCl 60° prism with base length $B=7.5\times 2$ cm, calculated values of W_n/W_1 as shown in Table I are obtained from Expression (2).

Table I. Calculated values of W_n/W_1 for the same values of signal-to-noise ratio

$\lambda(\mu)$	$n=2$	$n=3$
6	1.53	2.01
9	1.54	2.07
12	1.58	2.18
14	1.69	2.47

Table I shows that the same values of the signal-to-noise ratio are not obtained unless W_n/W_1 is made larger for longer wavelength, for the energy loss by the absorption of prism increases with the wavelength and with n.

Geometrical spectral width of the slit Δ is

$$\Delta_n \sim W_n/D_n . \qquad (3)$$

From Expression (2)

$$\Delta_n=(W_n/nW_1)\Delta_1 \qquad (4)$$

Resolving power Δ' of the prism is

$$\Delta_n'=(1/n)\Delta_1' \qquad (5)$$

In order to express the resolution of infrared spectrophotometer, if Brodersen's expression[6] is used and the width of absorption line is negligible, a measure of the resolution $\Delta\nu$ is

5) J. Strong: Phys. Rev. **37** (1931) 1661.
6) Svent Brodersen: J. Opt. Soc. Amer. **43** (1953) 877.

$$\Delta\nu_n^2=\Delta_n^2+\Delta_n'^2 \quad (6)$$

In practice, $\Delta\nu$ is the half of wave number difference of two closest adjacent lines to be separated.

From Expressions (4) and (5),

$$\Delta\nu_n^2=(1/n)^2\{(W_n/W_1)^2\Delta_1^2+\Delta_1'^2\} \quad (7)$$

Or,

$$\begin{aligned}\Delta\nu_1/\Delta\nu_n&=n/(W_n/W_1) && \Delta_1>>\Delta_1'\\ &=\sqrt{2}/[(1/n)^2\{(W_n/W_1)^2+1\}]^{1/2} && \Delta_1\approx\Delta_1'\\ &=n && \Delta_1<<\Delta_1'\end{aligned} \quad (8)$$

Using Table I, Table II is obtained from Expressions (8).

Table II. $\Delta_1/\Delta\nu_n$ for the same values of signal-to-noise ratio.

n	2			3		
Case / λ (μ)	$\Delta_1>>\Delta_1'$	$\Delta_1\approx\Delta_1'$	$\Delta_1<<\Delta_1'$	$\Delta_1>>\Delta_1'$	$\Delta_1\approx\Delta_1'$	$\Delta_1<<\Delta_1'$
6	1.31	1.55	2	1.49	1.90	3
9	1.30	1.54	2	1.45	1.85	3
12	1.27	1.51	2	1.39	1.79	3
14	1.19	1.45	2	1.22	1.60	3

If absorption and reflection losses by the prism are not considered, the resolution will increase from $\sqrt{n}$ to n times on all wavelength regions as Walsh[7] reported. But in practice, as shown in Table II, the increase of resolution in long wavelength region is considerably below $\sqrt{n}$ times in the case of $\Delta_1>>\Delta_1'$. On the other hand, since infrared energy in the long wavelength region is very weak, condition $\Delta_1<<\Delta_1'$ is not practical. Therefore, n times is only ideal. Moreover, it is considered that the resolution in longer wavelength region does not increase as shown in Table II. In order to obtain the same values of signal-to-noise ratio as in the case of single pass, a wide slit width as shown in Table I is necessary. However, the smaller the receiving area, the more sensitive the detector. If the slit is wide as shown in Table I, image of the slit may protrude from the receiver. Thus, full signal may not be obtained in the case of $n\geq 2$ in long wavelength region. For this reason, increase of n does not

7) A. Walsh: J. Opt. Soc. Amer. **42** (1952) 96.

always mean increase of resolution, or furthermore, spectrum may not be recorded because of the defficiency of energy.

b) Wavelength Scanning Speed

Wavelength scanning speed for the faithfull recording of spectrum should be decided under consideration of the response time, form of spectrum and slit width. Let us consider the case of recording the spectrum of one and the same sample by the single pass and by the double or multiple pass. From Expression (1), the available energy is proportional to the square of the slit width and inversely proportional to the angular dispersion. On the other hand, the response time, namely, the time in which the pen travels from 100% to 0% when the sample beam is intercepted, is inversely proportional to the available energy. That is, the smaller the response time is, the faster the pen will be. Therefore, fast scanning speed may be used when the available energy is large. With any spectrophotometers, to speed up the scanning and at the same time to obtain faithful recording, the slit must be widened which will, however, impair the resolution.

In the case of n traverses though prism, the slit width for the same resolution as that with single pass is n times. Therefore, the available energy corresponding to this slit width is

$$I_n = n\,(T_n F_n / T_1 F_1)\, I_1 . \qquad (9)$$

Thus, recording of spectrum with the same resolution as that with single pass is obtained by the scanning speed of $n\,(T_n F_n / T_1 F_1)$ times.

If the available energies are the same in these instruments the scanning speed also can be the same, but resolution increases as shown in Table II.

c) False Radiation

The radiation from the source enters monochromator directly or after through the sample, and a part of the light which is scattered by the surfaces of mirrors or prism enters the exit slit. Furthermore, when the spectrophotometer is set to nominal wavelength, the light of the region of wavelength shorter than nominal takes complex optical paths in the prism after the reflection by Littrow mirror, and finally together with the light of nominal wavelength enters the exit slit. The former is the scattered light, the latter the stray light. Since these false radiations strike the detector together with the radiation of nominal wavelength, transmittance is different from the true value. In longer wavelength region where the slit should be wide (in the case of NaCl prism, longer than 10 μ), the intensity of radiation entering monochromator is considerably high. Therefore,

at such a wavelength region the effect of false radiation may be expected not negligible. In general, the longer the wavelength, the larger the effect of false radiation.

When the spectrophotometer is set to long nominal wavelenth λ_0 and has the slit width s_0, let us assign the following notations for the purpose of examining the effect of false radiation.

U_0, u_0: light intensities of nominal wavelength λ_0 through reference and sample cells.

U_1, u_1: total intensities of source radiation which enter monochromator after through reference and sample cells, a few percent of each of these intensities plays the part of scattered light.

U_2, u_2: of the light through reference and sample cells, light intensities of shorter wavelength than $\lambda_0-\overline{\lambda}$, where $\overline{\lambda}$ is a constant. A few percent of each of these intensities plays the part of stray light.

α, β: coefficients of scattered and stray lights.

Fig. 1 shows these correlations.

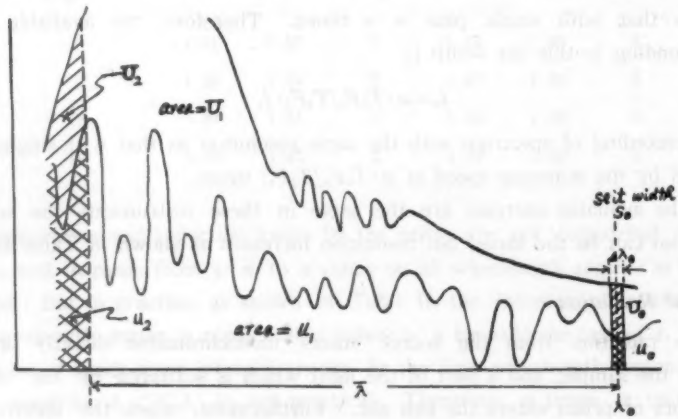

Fig. 1. Schematic diagram showing the energy distributions of light through reference (upper curve) and sample cells (lower curve) when spectrophotometer is set to long nominal wavelength λ_0.

When the false radiation is not present, transmittance at λ_0 is

$$T_0=u_0/U_0\,. \tag{10}$$

However, if the false radiation is present, the transmittance will be indicated by $T=T_0+\Delta T$. In such a case, it is obvious that

$$T(U_0+\alpha U_1+\beta U_2)=u_0+\alpha u_1+\beta u_2 \ . \tag{11}$$

In order to be a serviceable instrument, conditions of $U_0 >> \alpha U_1$ and $U_0 >> \beta U_2$ must be satisfied. Further, if we put

$$u_1/U_1=T_1 \quad \text{and} \quad u_2/U_2=T_2 \ , \tag{12}$$

from Expression (11),

$$\Delta T=(1/U_0)\{\alpha(T_1-T_0)U_1+\beta(T_2-T_0)U_2\} \tag{13}$$

which tells us that

(1) When identical samples are placed in both beams, $T_0=T_1=T_2=1$. Therefore, $\Delta T=0$. That is, 100% line is straight without the effect of false radiation.

(2) When the sample beam is intercepted, $T_0=T_1=T_0=0$. Namely $\Delta T=0$. This means that, since the effect of false radiation is absent, the pen remains on 0% line of recording paper.

(3) When the sample is placed in the sample beam and $T_0=0$ at λ_0,

$$\Delta T_l=(1/U_0)(\alpha T_1 U_1+\beta T_2 U_2) \tag{14}$$

Namely, the pen which should move to 0% stops at $100\,\Delta T_l$%. Since U_1, U_2, u_1 and u_2 are mostly governed by the light energies of short wavelength region from 2 to 6 μ, T_1 and T_2 do not change much even if LiF or CaF_2 plate together with the sample is placed in sample beam. Thus, we can experimentally measure ΔT_l. If LiF or CaF_2 plate alone is placed in sample beam, approximately $T_1=T_2=1$. The result becomes

$$(\Delta T_l)_{max}=(1/U_0)(\alpha U_1+\beta U_2) \tag{15}$$

$(\Delta T_l)_{max}$ is the maximum error at 0%, which is a quantity that can be measured experimentally.

(4) When the sample is placed in the sample beam, if $T_0=1$ at λ_0. Then,

$$\begin{aligned}\Delta T_u&=(1/U_0)\{\alpha(T_1-1)U_1+\beta(T_2-1)U_2\}\\&=\Delta T_l-(\Delta T_l)_{max} \ . \quad (<0)\end{aligned} \tag{16}$$

Using this expression, the error ΔT_u at 100% can be made known.

(5) Since ΔT is inversely proportional to the light intensity U_0 of wavelength λ_0 to which the spectrophotometer is set, the smaller the available energy, the larger the effect of false radiation. This is the reason that the effect of false radiation becomes apparent in long wavelength region.

For the reason mentioned above, when false radiation is present, the pen indicates $100\Delta T_l$% instead of true 0% and $100\,(1-\Delta T_u)$% instead of true 100%.

Quantities α and β are affected by optical arrangement of the instrument. α is also affected by diaphragms, blur of reflecting mirrors and surfaces of prism. But if full attention is paid it can be made $\alpha=0$.

When the effect of false radiation is not negligible, wavelength and transmittance of absorption line must be corrected. Since wavelength of absorption line is shifted towards shorter wavelength by the effect of false radiation, true wavelength is determined by extrapolation to zero concentration using the result of measurements for various concentrations. As seen from Fig. 2, true transmittance is obtained by the following expression.

$$T_0=(T-\Delta T_l)/\{1-(\Delta T_l)_{max}\} \quad \Delta T_l \leq T \leq 1+T\Delta_u \qquad (17)$$

where, $$(\Delta T_l)_{max}=\Delta T_l-\Delta T_u.$$

If the absorption of the sample is weak, ΔT_u is very small and may be ignored.

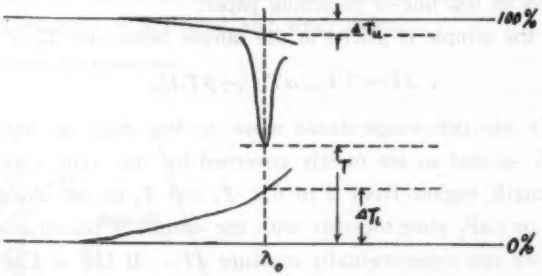

Fig. 2. Effect of false radiation on the true value of percent transmission.

When the instrument is operated in a long wavelength region, in order to be free from the correction mentioned above, we must decrease or eliminate the quantities U_1, U_2, u_1 and u_2 by instrumentation. This is done

(1) by excluding the light of the shorter wavelength region using a filter placed in common optical path of both reference and sample beams.

(2) by letting the dispersed light into monochromator using a fore prism.

Unlike the case with single beam type instrument, it is difficult to chop only the necessary light with double or multiple pass type using one monochromator. Therefore, when such instrument is used, there is no means other than making correction by calculation or using a filter. As to the effect of false radiation of double beam double or multiple pass, it will be dealt with later. The use of fore prism is, after all, the use of double monochromator. Although the false radiation from the first monochromator enters the second, it is either re-

dispersed and does not enter the exit slit or becomes so feeble by being scattered so that it can be neglected. As there is no perfect filter, use of double monochromator is no doubt of advantage in eliminating the effect of false radiation.

3. Constructed Infrared Spectrophotometers

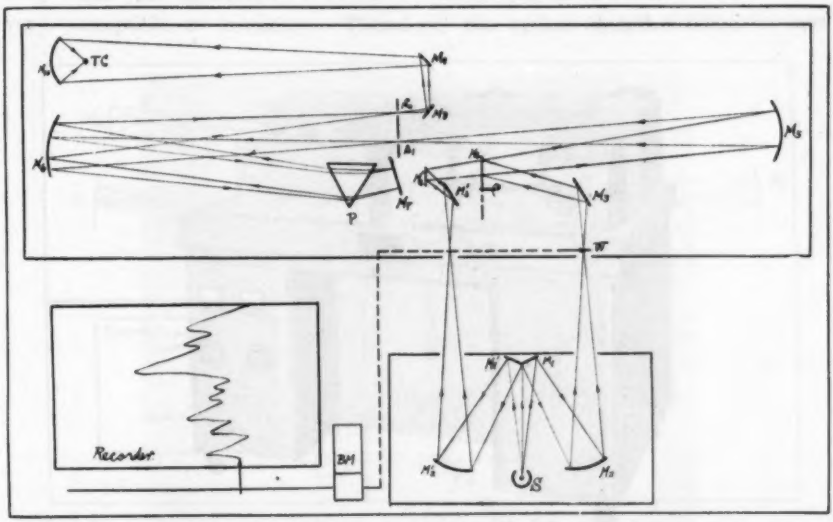

Fig. 3. Optical arrangement of double beam single pass infrared spectrophotometer. S, radiation source; S_1, S_2, entrance and exit slits; P, Prism; TC, detector; M_i (i=1, 2, ···, 10), plane or concave mirror; W, optical wedge; BM, control motor.

For the construction of new spectrophotometers, components of the previously reported single pass double beam infrared spectrophotometer[3] such as the double beam system, the detector and the electric system were utilized. Only the monochromator and the rest of the optical system were modified. The following four were constructed by way of experimentation.

(a) Double beam double pass infrared spectrophotometer.
(abbreviation: DB-DP infrared spectrophotometer)

(b) Double beam triple pass infrared spectrophotometer.
(abbreviation: DB-TP infrared spectrophotometer)

(c) Double beam double monochro infrared spectrophotometer in which each monochromator is of single pass.
(abbreviation: DB-DM-SS infrared spectrophotometer)

(d) Double beam double pass double monochro infrared spectrophotometer in

which 1st monochromator is of single pass and the 2nd is of double pass. (abbreviation: DB-DM-SD infrared spectrophotometer)

Since these instruments were designed to be of the same appearance as shown in Fig. 4, which is the single pass type, all look alike. The optical system was modified and improved as the construction progressed from one type to another. For later comparison, NH_3 spectrum recorded in 1.8 min/μ by the single pass type is shown in Fig. 5.

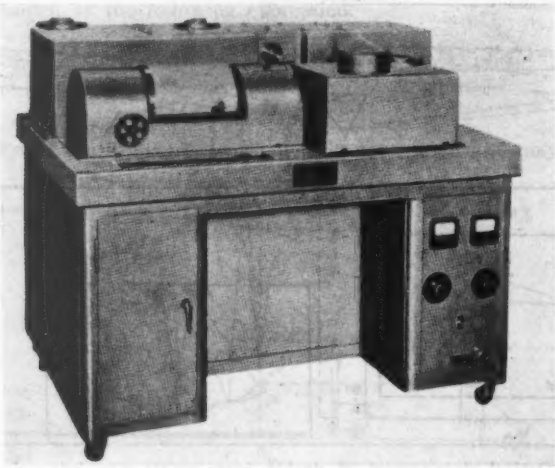

Fig. 4. Automatic recording double beam infrared spectrophotometer.

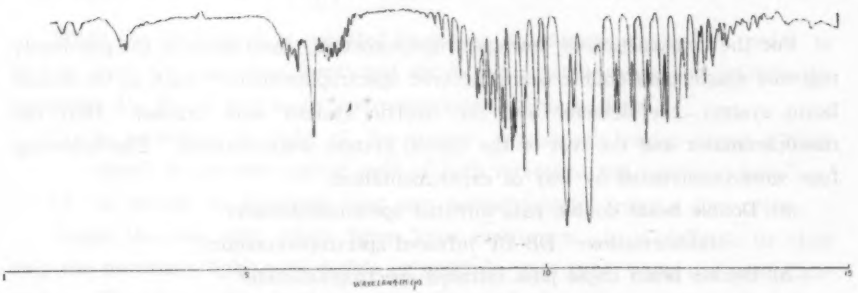

Fig. 5. *NH_3* spectrum recorded by double beam single pass infrared spectrophotometer. Scanning speed. 1.8 min/μ.

(a) DB-DP *infrared spectrophotometer*

As for the DB-DP in which one prism is utilized twice, a few papers have

been published[8)-12)]. The author also performed an experiment using the optical arrangement as shown in Fig. 6. The instrument with this optical arrangement is free from false radiation as Walsh's single beam type, but in order to increase the resolution in short wavelength region, windows of sample cell needed be optically plane and kept clear which is however difficult to obtain since many materials transmitting infrared rays are hard to polish optically plane and are very susceptible to humidity. Therefore, the optical system of Fig. 6 is un-

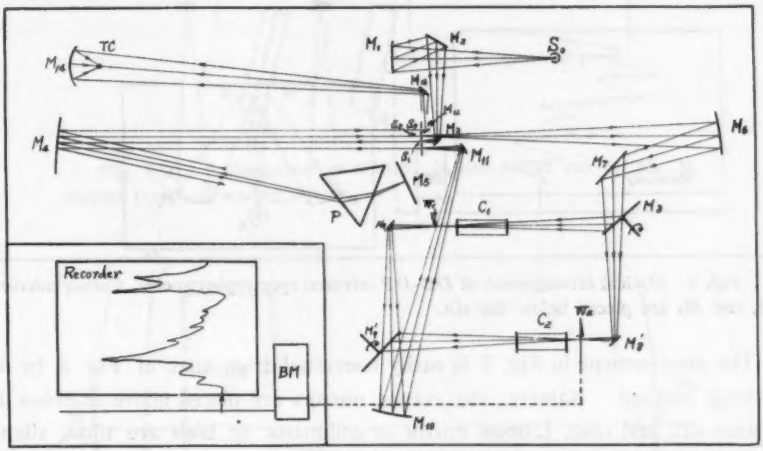

Fig. 6. An example of optical arrangement for *DB-DP* infrared spectrophotometer.

suitable to infrared spectrophotometer. Thus, an arrangement as shown in Fig. 7 was adopted.

The arrangement around the corner mirrors M_8 and M_9 is that suggested by Rochester and Martin[13)]. Namely, the 1st spectrum is reflected towards collimator by the corner mirror placed above the entrance slit jaws.

Recently Cole[8)] applied this method to single beam double pass type and merely suggested that satisfactory working of DB-DP using this method would be possible. But, since the DB-DP type was not actually constructed, he did not go into detail. Therefore, as the first step of the study, the author constructed this type and examined its various performances.

8) A. R. H. Cole: J. Opt. Soc. Amer. **43** (1953) 807.
9) S. F. D. Orr: J. Opt. Soc. Amer. **45** (1953) 709.
10) J. Pliva: Jl. Sci. Instrum. **31** (1954) 434.
11) The Perkin Elmer Instrument News **7** No. 3 (1956) 7.
12) K. Kudo: Science of Light **5** (1956) 1.
13) J. C. O. Rochester and A. E. Martin: Nature **168** (1951) 785.

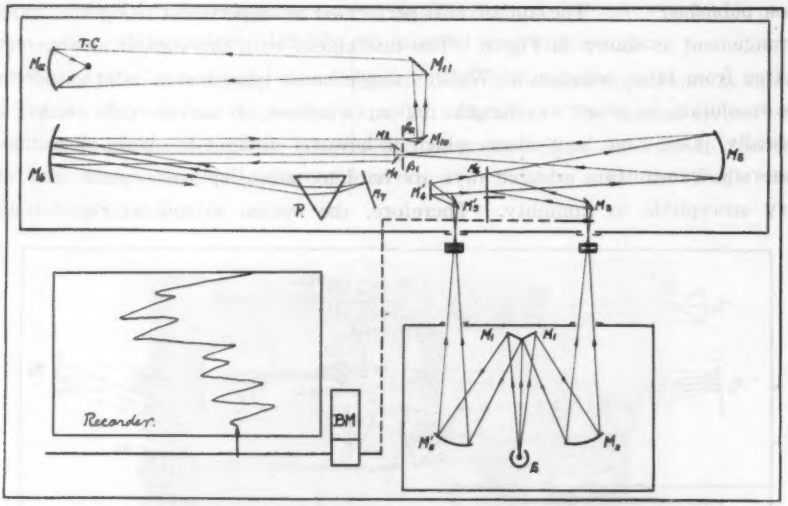

Fig. 7. Optical arrangement of *DB-DP* infrared spectrophotometer. Corner mirrors M_8 and M_9 are placed below the slit.

The arrangement in Fig. 7 is easily converted from that of Fig. 3 by the following method. Namely, the corner mirrors are placed above or below the entrance slit, and next, Littrow mirror or collimator or both are tilted slightly so that the 1st spectrum strikes the corner mirrors. The corner mirrors are also tilted slightly so that the reflected 1st spectrum is projected on the full surface of the prism.

In general, the image of the straight entrance slit formed by the 1st mo-no chromator (single pass) is paraboloidal. If the image of the center of the slit is shifted below the slit by the slit length, it will be approximately on the parabola while the rest of the image is not. However, if the angle which the slit subtends at the center of collimator is small, the curvature of the image will be nearly equal to that in single beam double pass type. This can be made clear by calculation. In the present case, difference of slit curvatures in *DB-DP* and single beam double pass types could not be found.

However, since the upper side of entrance slit corresponds to the lower side of image and ***vice versa***, aberration of image becomes large in proportion to the distance from the center of entrance slit.

If a curved entrance slit is used, the image formed by the 1st monochromator is approximately straight even at green light, and tilted to the principal plane of prism as seen from Fig. 8 (a). So, the resolution does not increase

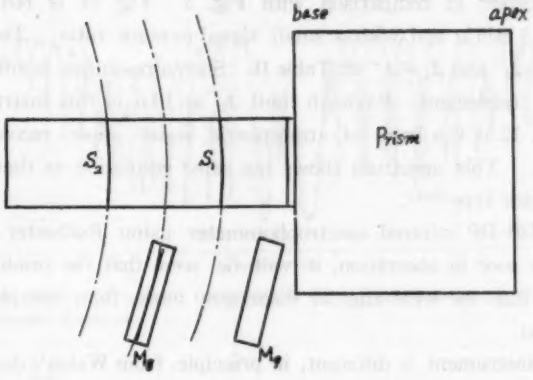

Fig. 8 (a). Arrangement of slits S_1, S_2 and corner mirror M_8, M_9 viewed from collimating mirror.

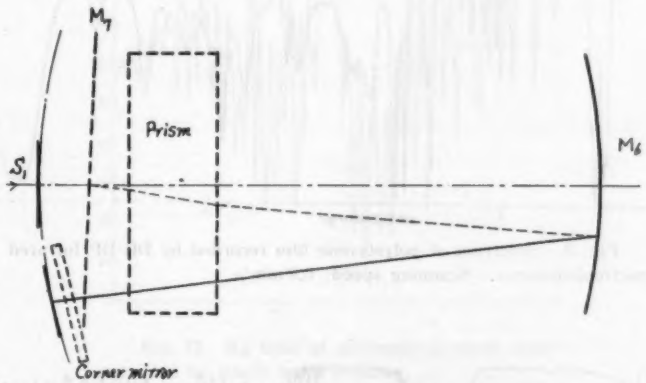

Fig. 8 (b). Side view of corner mirror. In order to form the image of slit below the slit, Littrow mirror M_7 must be tilted slightly.

unless the image by the 2nd monochromator is made parallel to exit slit by tilting corner mirrors. Next, as seen from Fig. 8 (b), the image by the 1st monochromator is formed at focal plane of the collimator. Therefore, in order to maximize the energy of light for the 2nd spectrum, corner mirror should be tilted slightly upward. These adjustments are easily performed by watching the reflecting light at the surface of the prism.

Figs. 9 to 12 are spectra recorded by this instrument. Fig. 9 is the spectrum of polystyrene film recorded with scanning speed 0.9 min/μ, the resolution near 3.3 μ is worthy of note. Fig. 10 is NH_3 spectrum recorded with 1.8 min/μ, the

resolution is better in comparison with Fig. 5. Fig. 11 is NH_3 10.5 μ band recorded with 5 min/μ and with a small signal-to-noise ratio. The resolution is between $\Delta_1 >> \Delta_1'$ and $\Delta_1 \approx \Delta_1'$ of Table II. Such a resolution is difficult to obtain by single pass instrument. Rayleigh limit Δ_2' at 10 μ in this instrument is about 0.5 cm^{-1}. Fig. 12 is 6 μ band of atmospheric water vapor recorded by single beam working. This spectrum shows the same resolution as that of the single beam double pass type[14)15)].

Although DB-DP infrared spectrophotometer using Rochester and Martin's arrangement is poor in aberration, it will be seen that the resolution increases for the reason that the wide angular dispersion more than compensate for the large aberration.

Since this instrument is different, in principle, from Walsh's double pass type,

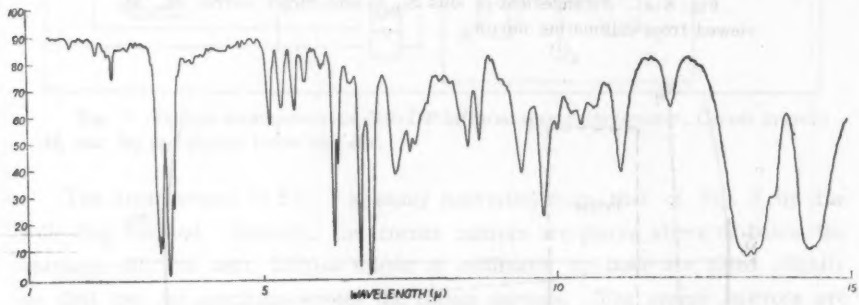

Fig. 9. Spectrum of polystyrene film recorded by DB-DP Infrared spectrophotometer. Scanning speed; 0.9 min/μ.

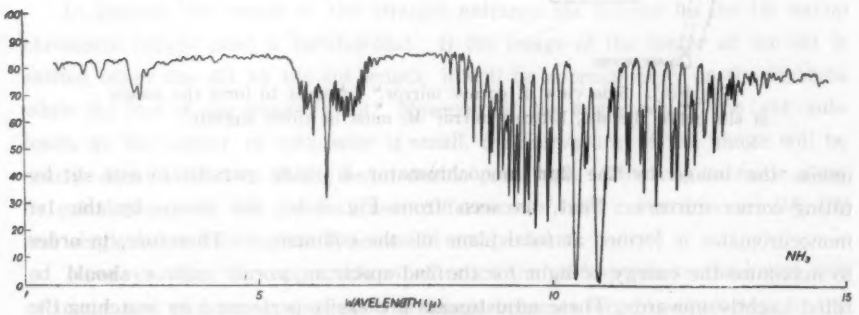

Fig. 10. NH_3 spectrum recorded by DB-DP infrared spectrophotometer. Scanning speed; 1.8 min/μ.

14) K. Kudo and T. Miyazaki: J. of Applied Physics. Japan. **24** (1955) 461.
15) A. Walsh: J. Opt. Soc. Amer. **42** (1952) 96.

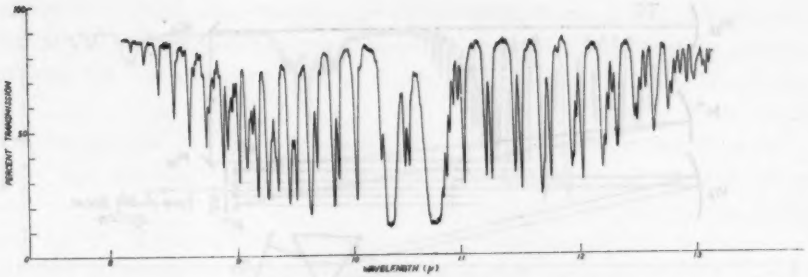

Fig. 11. NH_3 10.5 μ band recorded by DB-DP infrared spectrophotometer. Scanning speed; 5 min/μ.

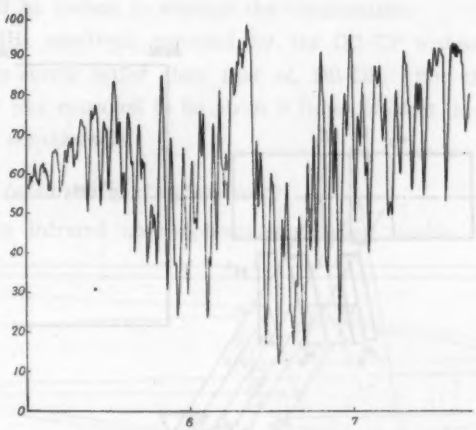

Fig. 12. 6 μ band of atmospheric water vapor recorded by single beam working.

the effect of false radiation is surely present. Even if the signal-to-noise ratio equals to that of the single pass type, the slit width is 1.7 times of the latter at 14 μ. Therefore, radiation energy that enters monochromator is 1.7^2 times and the effect of false radiation is expected to be about 3 times. Actually, this effect was about 7% and 16% at 14 and 15 μ respectively. By using a filter, this effect was weakened to about 5% at 15 μ.

(b) DB–TP *Infrared Spectrophotometer*

Cole mentioned that Rochester and Martin's principle could not be used for multiple pass, but it is not always impossible. If the three mirrors M', M'' and M''' as shown in Figs. 13 and 14 are added to Fig. 7, triple pass can be realized.

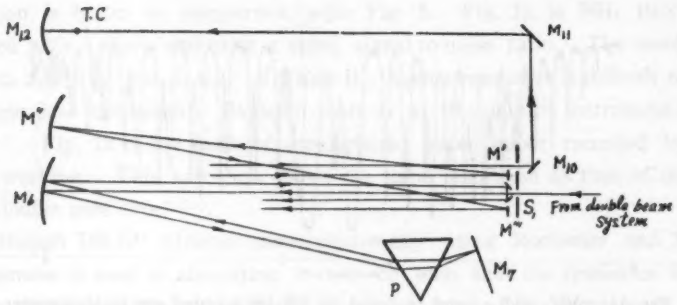

Fig. 13. Optical arrangement of DB-TP infrared spectrophotometer. By three mirrors M', M'', M''' 2nd spectrum is reflected towards collimator.

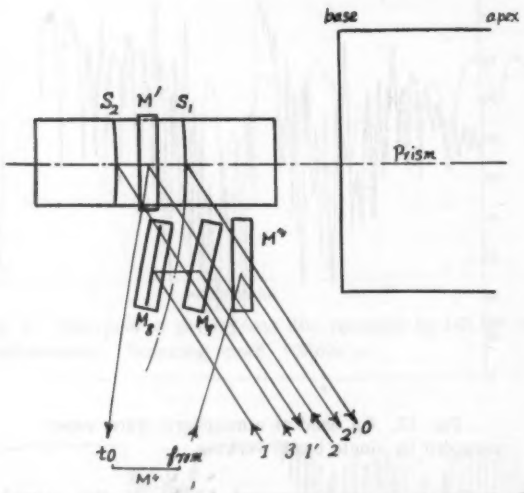

Fig. 14. Schematic diagram showing the arrangement of slits S_1, S_2, corner mirrors M_8, M_9 and attachment mirrors M' and M'''.

Namely, the 2nd spectrum is reflected by the small plane mirror M' towards the spherical mirror M'' which projects the spectrum to the plane mirror M''' positioned at the same height as the corner mirrors and M''' reflects this light towards the collimator. It this case, the area of reflecting surface of the corner mirror M_8 must be restricted so as to avoid the overlapping of the order of spectra.

Quadruple pass would be realized by the application of this method, but it is very difficult to adjust even the triple pass, moreover the aberration will be

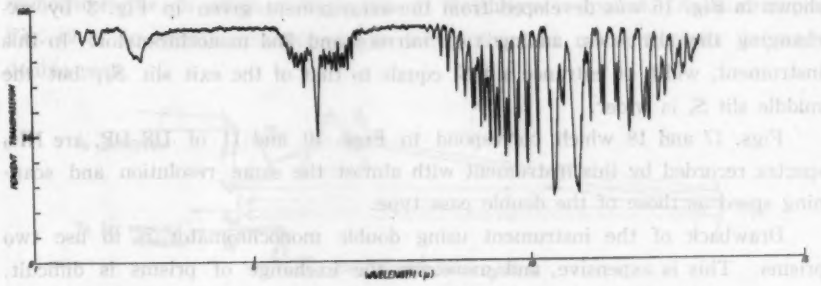

Fig. 15. NH_3 spectrum recorded by DB-TP infrared spectrophotometer. Scanning speed 1.8 min/μ.

large. So it will be useless to attempt the construction.

Fig. 15 is NH_3 spectrum recorded by the DB-TP without full adjustment. The resolution is surely better than that of DB-DP. But the effect of false radiation, which was expected to be about 9 times of that in single pass types, was found quite considerable.

(c) DB-DM-SS *Infrared Spectrophotometer*

Double beam infrared spectrophotometer using double monochromator as

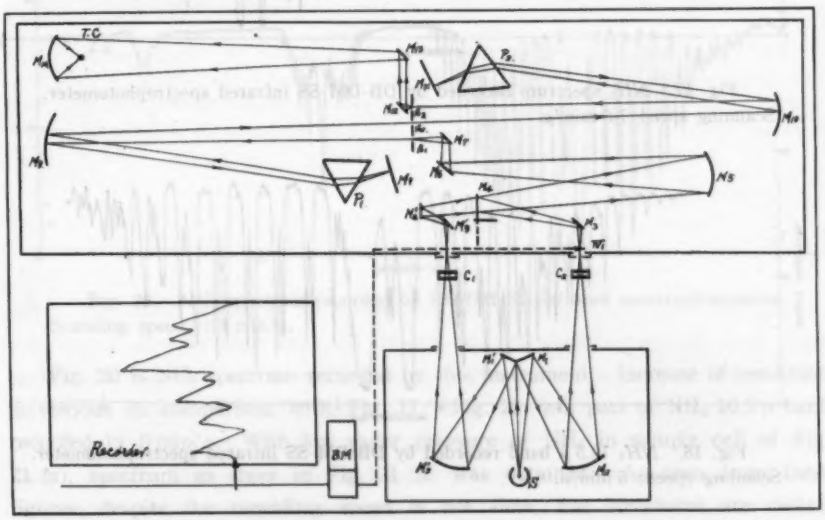

Fig. 16. Optical arrangement of DB-DM-SS infrared spectrophotometer. Plane mirrons M_6, M_7, slit jaws S_1, S_2, S_3 and 2nd monochromator which includes collimator M_{10}, Prism P_2 and Littrow mirror M_{10} are supplemented to double beam single pass infrared spectrophotometer.

shown in Fig. 16 was developed from the arrangement given in Fig. 3 by exchanging the slit jaws, adding two mirrors and 2nd monochromator. In this instrument, width of entrance slit S_1 equals to that of the exit slit S_3, but the middle slit S_2 is wider.

Figs. 17 and 18 which correspond to Figs. 10 and 11 of DB-DP, are NH_3 spectra recorded by this instrument with almost the same resolution and scanning speed as those of the double pass type.

Drawback of the instrument using double monochromator is to use two prisms. This is expensive, and moreover the exchange of prisms is difficult. But, as mentioned previously, the false radiation is not present. Therefore, in order to realize a double beam multiple pass, no other methods are conceivable than employing double monochromator.

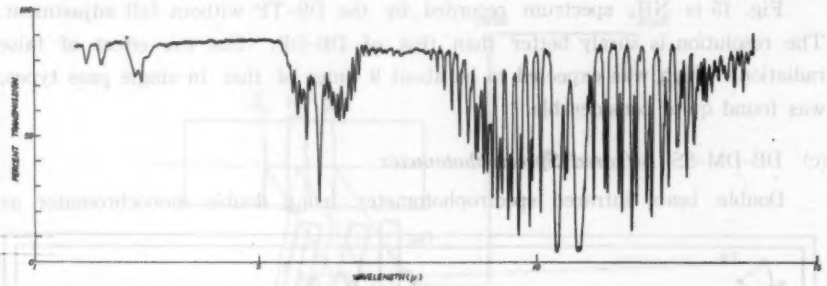

Fig. 17. NH_3 spectrum recorded by DB-DM-SS infrared spectrophotometer. Scanning speed 1.8 min/μ.

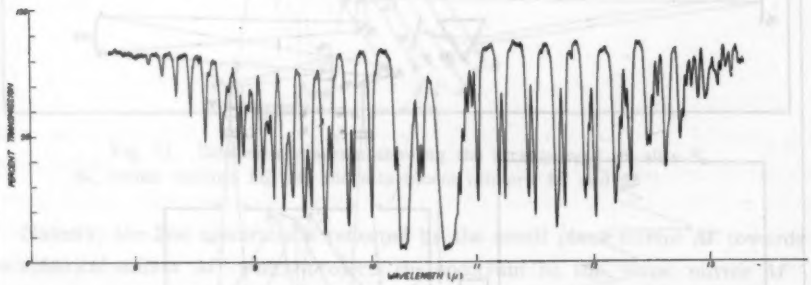

Fig. 18. NH_3 10.5 μ band recorded by DB-DM-SS infrared spectrophotometer. Scanning speed; 5 min/μ.

(d) DB-DM-SD *Infrared Spectrophotometer*

It is easy to construct multiple pass by means of double monochromator. Namely, only the 1st order radiation in the 1st monochromator enters the 2nd

monochrometer, in which multiple pass of Walsh type is applied. As an example, Fig. 19 is an optical arrangement in which the 2nd monochromator is made double pass.

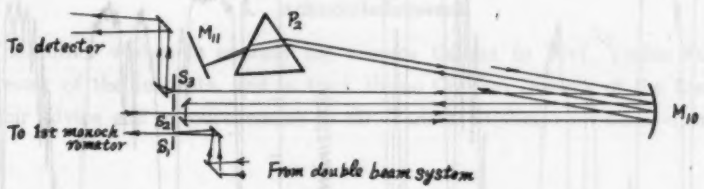

Fig. 19. Using double monochromator, multiple pass is easily constructed. This arrangement shows double pass in the second monochromater.

If the radiation is dispersed n times by the prism P_2 and if the width of the slit S_2 is s_2, the distance between S_2 and S_3 should be more than $(3n-1)\,2^{n-3}s_2$ otherwise, spectra of different orders will be overlapped.

If the 2nd monochromator is made double pass, the available energy in long wavelength region will be very weak for the reason mentioned previously. Thus, with NaCl prisms, the reproducibility in the wavelength region longer than 14.5 μ was not satisfactory. This will be improved by using KBr prisms.

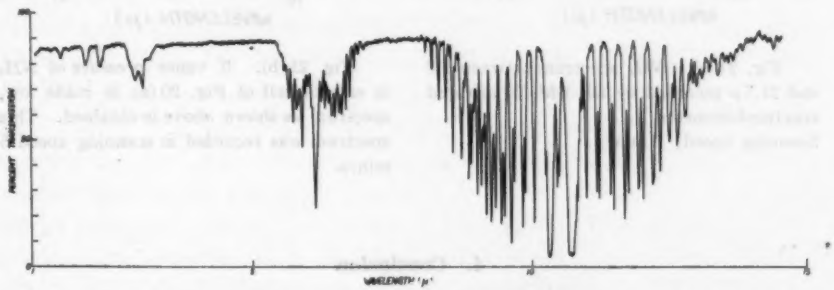

Fig. 20. NH_3 spectrum recorded by DB-DM-SD infrared spectrophotometer. Scanning speed; 1.8 min/μ.

Fig. 20 is NH_3 spectrum recorded by this instrument. Increase of resolution is obvious in comparison with Fig. 17. Fig. 21 is a part of NH_3 10.5 μ band recorded in 5 min/μ. With low vapor pressure of NH_3 in sample cell of Fig. 21 (a), spectrum as show in Fig. 21 (b) was obtained. As seen from these figures, despite the recording speed is not slow, fine structures are clearly recorded. If narrower slit and slower scanning speed are used, still better resolution will be obtained. In this type, it is natural that false radiation is not present.

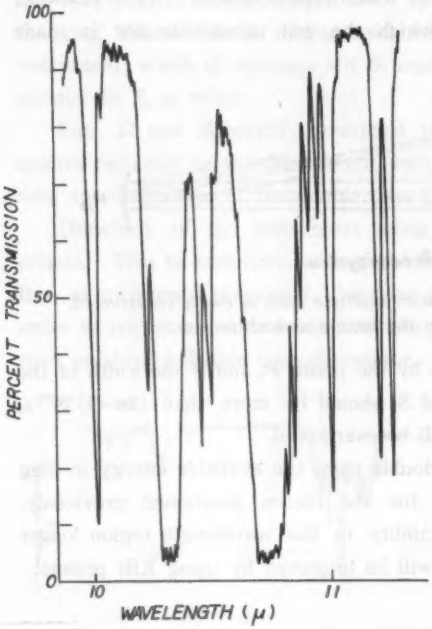

Fig. 21 (a). NH_3 spectrum between 9.8 and 11.5 μ recorded by DB-DM-SD infrared spectrophotometer.
Scanning speed; 5 min/μ.

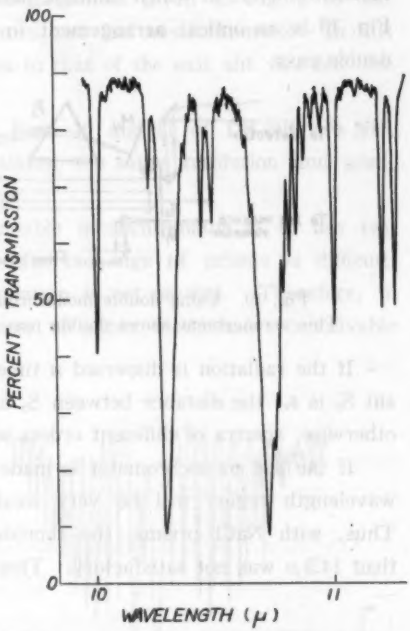

Fig. 21 (b). If vapor pressure of NH_3 in sample cell of Fig. 20 (a) is made low, spectrum as shown above is obtained. This spectrum was recorded at scanning speed 5 min/μ.

4. Conclusion

For increasing the resolution and shortening the recording time, any of the above methods can be used. But, as regards the false radiation, it is inherent in double or multiple pass type and can not be eliminated. To weaken its effect, filters (transmission or reflection) have to be used. However, there is no perfect filter without the loss of energy to nominal wavelength and any attempt to render the false radiation negligible will inevitably weaken the available energy. And again, widening of slit to augment the energy lowers the resolution. From this reason, DB-DP, which has comparatively small effect of false radiation, can be a practical instrument but not DB-TP.

In the case of double monochromator, since the 1st monochromator is an

ideal filter, multiple pass can be constructed without false radiation and it will be an ideal instrument as infrared spectrophotometer.

5. Acknowledgement

The author wishes to express his sincere thanks to Prof. Yoshio Fujioka, ex-Director of the Institute, and to Prof. Haruo Ootuka, Director of the Institute, for their advice and encouregement to Mr. Tadashi Miyazaki for his co-operation.

An Example of Making a Bright Grating and its Application

Yoshimi SAKAYANAGI
Institute for Optical Research, Tokyo University of Education

(Received October 8, 1956)

Abstract

Ruling of grating on a non-metalic surface is described. Gratings that are ruled on surfaces other than those of metals can be made bright by vacuum evaporation method. Using fish glue for photographic printing affixed on glass, a bright grating is obtained. When this grating is used as transmission grating, zero order is scarcely seen. It can be used as a focusing glass. Replicas are obtained.

1. Introduction

For making a bright grating, control of the shape of groove is essencial, but in practice, it is by no means easy. Among the shapes of groove, echelette is practical and suited for concentration of energy[1]. But even this simplest form is not easy to be cut in an ideal form. Polishing of the diamond edge and selection of the grating material are also necessary for good grooves to be ruled.

As for the material, speculum metal has commonly been used. But the metal is hard and brittle, and good bright gratings are made only when a good diamond edge is found by sheer chance. However, bright gratings are now made on thickly vacuum evaporated aluminium film with a well polished diamond edge[2]. Here again, another problem is the art of polishing. For ruling for far infrared, polishing of diamond edge presents no great difficulty. But when it comes to the material, soft metal such as copper requires special attention. Recently, a very soft metal, an alloy of lead and tin, is being used with unpolished surface on which the ruling is made by keeping the diamond edge at a fixed height[3]. This technique is so far favorable for wide spaced ruling such as on far infrared grating but for ordinary ones success is doubtful.

Lately, the writer was asked to make a grating of 180–200 lines/mm, very weak in zero order and very strong in the first order spectrum on one side.

1) H. A. Rowland: Phil. Mag. **35** (1893) 397.
2) R. W. Wood: J. Opt. Soc. Amer. **34** (1944) 509.
3) Private communication from Prof. H. Yoshinaga.

Since there was a difficulty in preparing aluminium film which is thick enough for this purpose, a non-metal surface was tried.

2. Ruling

Good grooves can be ruled not by cutting but by deforming. Therefore speculum metal is recently replaced by evaporated aluminium film on glass. As the ruled surface can be later metal evaporated, any non-metal surface is expected to be used for the purpose. After repeated tests, fish glue for photographic printing was found to meet the requirements.

The composition of the glue is as follows:

Ammonium dichromate	1 g
Fish glue	10 c.c.
Water	20 c.c.

The solution after filtration is left standing for 3–4 days, then poured evenly on a clean glass plate which is rotated to remove excess glue by the centrifugal force. The plate is then dried on a heater. The film becomes stronger by being exposed to the sun for approximately ten minutes. If the solution is used immediatly after the preparation, a film can be made so thin that the interference colour becomes observable, but the film is preferred not too thin for the present purpose. The polishing of the diamond edge was undertaken by the Tokyo Diamond Co. where diamond points for the use of micro hardness tester are being made.

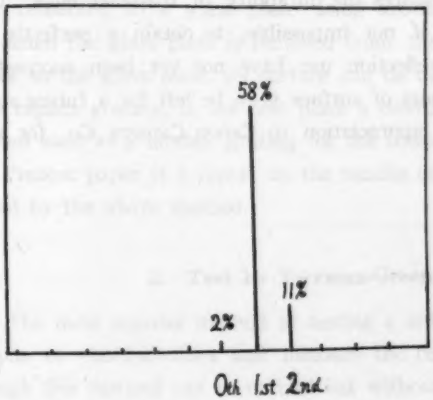

Fig. 1.

Fig. 2.

Gratings of 180–240 lines/mm were made. The intensity distribution by one of them used as transmission grating is illustrated in Fig. 1. The weakness of

zero order is apparent. Fig. 2 is a photograph of a line taken direct (top half) and through the grating (bottom half), the line being placed close to the grating. The zero order line, which should be the continuation of the line seen at the top, is hardly perceptible.

The same is the case of a line formed as an image by a lens. As shown in Fig. 3, the image is shifted right or left according as the grating is placed inside or outside the focus. Thus a focusing glass can be made by using the grating as its bottom half[4]. The position of the grating where the images at top and bottom join in one straight line is the focal plane. It is also possible to obtain replicas from the grating after aluminizing the surface.

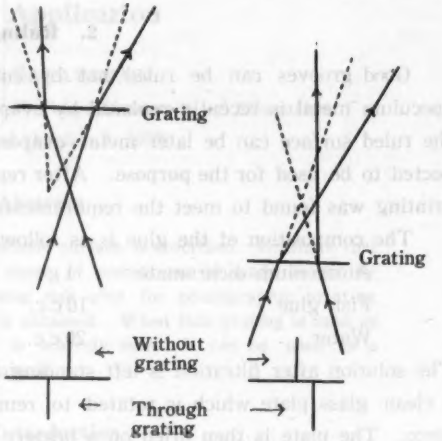

Fig. 3.

3. Conclusion

As fish gule is soft and can easily be deformed, it is not only convenient for making bright grating but also assures the durability of diamond edge. Only disadvantage is that it is difficult, if not impossible, to obtain a perfectly flat surface. Therefore gratings for reflection use have not yet been successfully produced. Acquisition of the flatness of surface is to be left for a future study.

Writer wishes to express his appreciation to Canon Camera Co. for their kind assistance.

4) Patent (Japan) No. 30-9474.

Production of Replica Gratings II

Masao SEYA and Katsuya GOTO
Institute for Optical Research, Tokyo University of Education

(Received October 1, 1956)

Abstract

In the previous paper the method and the technique of the production of replica gratings by the evaporation method are reported. Present paper is the report on the test of the replica gratings by interferometric method and the energy distribution of diffracted light of various orders.

1. Introduction

Recently there is a great demand for diffraction grating as an optical equipment, but as the technique of its production involves high precision, the gratings are expensive. To make it inexpensive, there is the prospect of producing replica gratings in large quantities for which several methods have been reported in the last fifty years, but detailed account for making good replica gratings has not so far been made known. The evaporation method was studied by the authors and the precise account of the method was published as Part I[1]. The outline of the method is as follows.

The original grating is at first coated with aluminum film by evaporation, then cemented to a glass plate using artificial resin. When polymerization is completed the glass plate is removed from the grating. As the aluminum film sticks to the glass plate, its surface can be used as grating. To produce a concave replica grating, in the first place a convex replica grating is made, which is then used as a mother grating for the concave replica grating.

Present paper is a report on the results of tests of the replica gratings produced by the above method.

2. Test by Twyman-Green Interferometer

The most popular method of testing a diffraction grating is to take photographs of spectral lines and measure the resolving power of the grating. Although this method can be carried out without any special apparatus, it is very difficult to tell where the imperfection is located and how it appears.

1) M. Seya and K. Goto: Science of Light **5** (1956) 2.

In the previous paper, results of observation by photographic method are given. But, since the difference in spectra taken with an original and replica gratings is not discernible on photographs, interferometric method using Twyman-Green interferometer was adopted for the comparison. Although this method is not new[2], its details were recently described at length by G. Stroke[3]. In Fig. 1, C is a collimater lens and I is a pinhole. The pinhole is illuminated by green light (5461A) of a mercury lamp filtered by interference filter. The light which comes out of the collimater lens is perfectly parallel. P is a half silvered plane parallel plate, R is a plane reference mirror and G is a grating. The direction of the grooves is set vertical. S is a convex lens and L is a camera which is focussed on the grating surface.

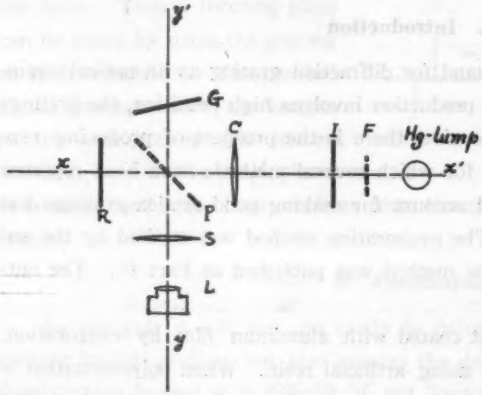

Fig. 1

In the first place the grating surface is set perpendicularly to the direction yy'. If the grating surface is perfectly flat, there will be observed equal thickness fringes on the surface of the grating, and all of the fringes will be straight, parallel and equally spaced. But if the grating surface is not good, the fringes will be curved and appear in various patterns. In this case irregularities of the grooves have no effect.

In the second place the grating is so set that the first order of green light diffracts to the direction of yy'. In this case the anomaly of the interference fringes show the existence of defect in the wave surface of the diffracted light and this defect is caused by imperfection of the grating surface and irregularities of the ruling. If the flatness is perfect and ruling is also perfect, there will appear straight and equally spaced fringes. Fig. 2 is the first order fringes of the original grating, and Figs. 3 and 4 are the zero and the first order fringes of a replica grating.

The size of the gratings is 50×35 mm and the number of grooves is about 600/mm. The fringes of the replica are a little worse than those of the original and further efforts are being made for the improvement.

2) C. Candler: Modern Interferometers. Hilger and Watts (1951) p. 151.
3) G. Stroke: J. Opt. Soc. Amer. **45** (1955) 30.

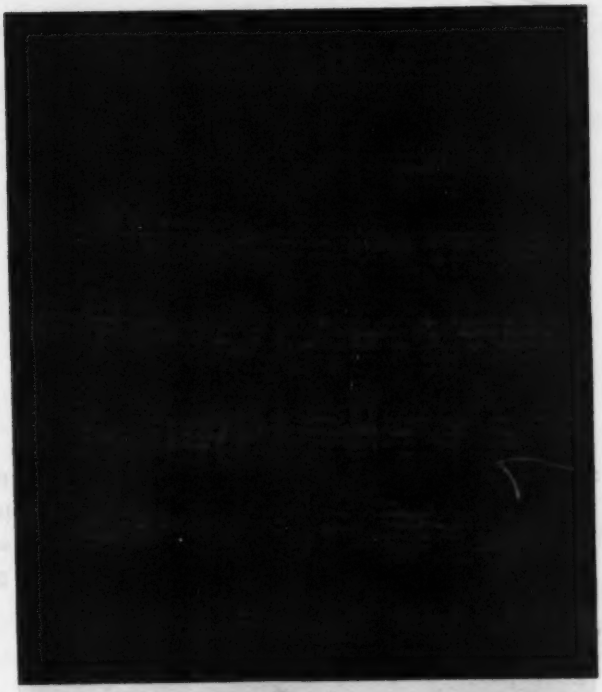

Fig. 2

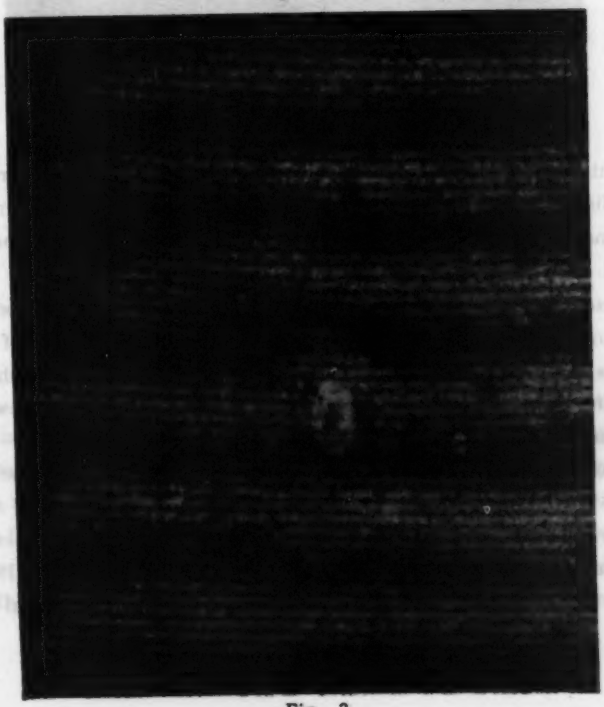

Fig. 3

Fig. 4

3. Test by Intensity Distribution

The interferometric method can tell nothing about the groove form. As the intensity distribution of diffracted light is affected by the groove form, the former was measured to examine whether the groove form of the original is truely reproduced.

The intensity distribution was measured by the following method. In Fig. 5, C is a collimator lens. The slit S_1 is illuminated by green light of a mercury lamp. G is the grating, L is a lens and M is a photomultiplier tube. In the measurement the multiplier tube was moved to and fro to obtain maximum response. S′ is a sector to change D.C. photo-current to A.C. current.

The incidence angles were 0 and 15 degrees. In the first place the intensities of the 0th, 1st, 2nd and the 3rd order spectra which appeared at one side of the grating normal were measured. In the case of normal incidence, the intensity of zero order can not be measured. Then the grating was rotated by 180° around the grating normal and the measurements were repeated. At normal incidence,

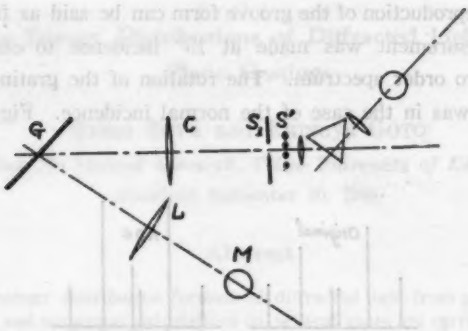

Fig. 5

the rotation of the grating makes the measurements be performed on both sides of the grating normal. Fig. 6 (a) shows the energy distribution at normal incidence, the abscissa being the order number of spectral lines and the ordinate the reading of photo-current.

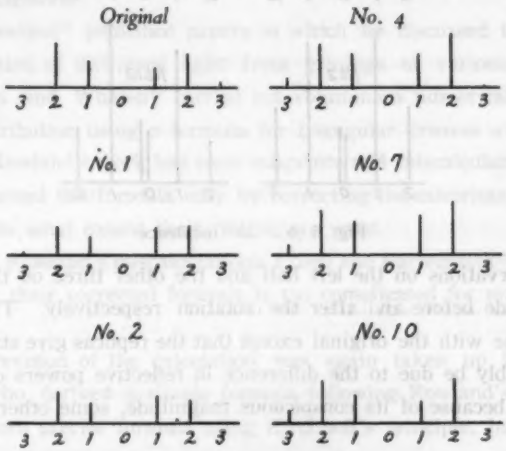

Fig. 6 (a). Normal incidence

Nos. 1, 4, 7 and 10 are the first replicas and No. 2 the second the mother of which is No. 1. All of the first replicas were made from the same original grating which was ruled on speculum metal. The original seems slightly asymmetric and the second order of the green light is the strongest. There are some differences in the energy distributions among the first replicas which are due probably to the different conditions under which the polymerization of resin progressed. But the general feature of the distribution is nearly the same with the

original and the reproduction of the groove form can be said as fairly satisfactory.

Another measurement was made at 15° incidence to examine the energy distribution of zero order spectrum. The rotation of the grating no longer had the import that was in the case of the normal incidence. Fig. 6 (b) shows the result.

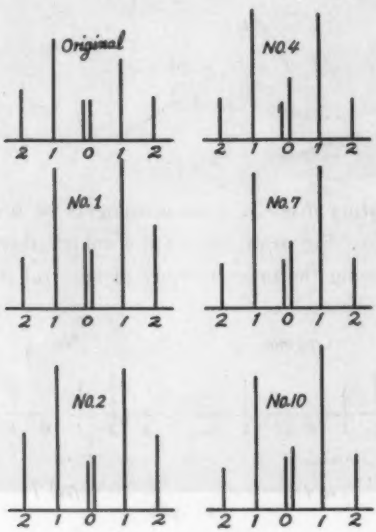

Fig. 6 (b). 15° incidence

Three observations on the left half and the other three on the right in each figure were made before and after the rotation respectively. The general feature is the same with the original except that the replicas give stronger intensity. This may probably be due to the difference in reflective powers of speculum and aluminum, but because of its conspicuous magnitude, some other causes are suggested.

4. The Aging of Replica Grating

It is still too early to refer to the question of aging, for even the oldest replica is only eight months old, during which period no change has been noticed. Detection of the effect, if any, will need a long time of observation.

On the Energy Distributions of Diffracted Light from Plane Gratings

Masao SEYA and Katsuya GOTO

Institute for Optical Research, Tokyo University of Education

(Received September 30, 1956)

Abstract

The energy distribution formula of diffracted light from plane gratings is derived and numerical calculations on several cases are carried out. The results and the calculations of Stumm and Whalen[1] are compared.

I. Introduction

The relations between the energy distribution of diffracted light and the groove form of plane gratings have been studied theoretically and experimentally by many investigators.

In 1893, Rowland[2] published papers in which he discussed theoretically the energy distribution of diffracted light from gratings of various groove forms. In 1946 Stamm and Whalen[1] carried out voluminous numerical calculations on the energy distribution using a formula for triangular grooves which was derived by Rowland. Rowland's work had some misprints and miscalculations and Stamm and Whalen revised the formula only by correcting the misprints. It is therefore hard to judge to what extent their results are valid.

Concerning Rowland's miscalculations, Friedl and Hartenstein[3], in 1955, pointed them out. But their corrected formula is too complicated for numerical calculations.

Recently, revision of the calculation was again taken up by Hatcher and Rohrbaugh[4] who derived a simple formula following Rowland's method. They also derived more precise formula using Kirchhoff's principle, but their calculations still involved some errors.

In this work, corrected and simplified formulae are derived by Rowland's method and by Kirchhoff's principle and numerical calculations are made for gratings of several types of triangular groove form.

1) R. F. Stamm and J. J. Whalen: J. Opt. Soc. Amer. **36** (1946) 2.
2) H. A. Rowland: Phil. Mag. (5) **35** (1893) 397.
3) W. Friedl and B. Hartenstein: J. Opt. Soc. Amer. **45** (1955) 398.
4) R. D. Hatcher and J. H. Rohrbaugh: J. Opt. Soc. Amer. **46** (1956) 104.

II. Derivation of Rowland's Formula

Rowland derived his formula considering only the phase difference of diffracted light from every point of the surface of the groove neglecting the inclination factor. Rowland's formula is read as follows.

$$I^2\left\{\frac{1+c^2}{(\mu-c\lambda)^2}\sin^2\frac{\pi u(\mu-c\lambda)}{l}+\frac{1+c'^2}{(\mu+c'\lambda)^2}\sin\frac{\pi(a-u)(\mu+c\lambda)}{l}\right.$$
$$+\frac{\sqrt{(1+c^2)(1+c'^2)}}{(\mu-c\lambda)(\mu+c'\lambda)}\sin\frac{\pi u(\mu-c\lambda)}{l}\sin\frac{\pi(a-u)(\mu+c'\lambda)}{l}$$
$$\left.\times\cos\frac{\pi}{l}[(\mu+c'\lambda)(a-u)-u(\mu-c\lambda)]\right\} \qquad \cdots\cdots(1)$$

where (see Fig. 1):

a, the grating constant.

l, the wavelength of light.

N, the order of spectrum (positive if on the side of zero order as incident beam, otherwise negative).

ϕ, the angle of incidence (always positive).

ψ, the angle of diffraction (positive if on the side of grating normal as ϕ, otherwise negative).

μ, $=\sin\phi+\sin\psi=Nl/a$.

λ, $=\cos\phi+\cos\psi$.

c, the slope of one side of the triangular groove, this side being expressed by the equation $x=-cy$ (c is positive).

c', the slope of the other side, this side being expressed by the equation $x=c'(y-a)$ (c' is positive).

u, the value of y at the intersection of the two sides.

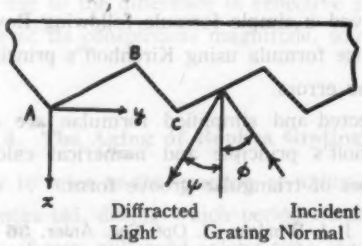

Fig. 1.

But, according to the authors' calculations this formula should be corrected as follows:

$$I^2\left\{\frac{1+c^2}{(\mu-c\lambda)^2}\sin^2\frac{\pi u(\mu-c\lambda)}{l}+\frac{1+c'^2}{(\mu+c'\lambda)^2}\sin^2\frac{\pi(a-u)(\mu+c'\lambda)}{l}\right.$$
$$+2\frac{\sqrt{(1+c^2)(1+c'^2)}}{(\mu-c\lambda)(\mu+c'\lambda)}\sin\frac{\pi u(\mu-c\lambda)}{l}\sin\frac{\pi(a-u)(\mu+c'\lambda)}{l}$$
$$\left.\times\cos\frac{\pi}{l}[(\mu+c'\lambda)(a-u)+u(\mu-c\lambda)]\right\} \qquad \cdots\cdots(2)$$

Using the next relation,

$$\frac{\pi(a-u)(\mu+c'\lambda)}{l}+\frac{\pi u(\mu-c\lambda)}{l}=N\pi \qquad \cdots\cdots(3)$$

(2) is reduced to a simple form

$$I^2\left[\sin\frac{\pi u(\mu-c\lambda)}{l}\right]^2\left[\frac{\sqrt{1+c^2}}{\mu-c\lambda}-\frac{\sqrt{1+c'^2}}{\mu+c'\lambda}\right]^2 \qquad \cdots\cdots(4)$$

(4) becomes indeterminate when $\mu=c\lambda$ or $\mu=-c'\lambda$. In these cases (4) reduces to

$$\pi^2u^2(1+c^2) \qquad \text{for} \quad \mu=c\lambda \qquad \cdots\cdots(5)$$

and

$$\pi^2(a-u)^2(1+c'^2) \qquad \text{for} \quad \mu=-c'\lambda \qquad \cdots\cdots(6)$$

Formulae (5) and (6) correspond to the blazed directions.

III. Derivation by Kirchhoff's Principle

Hatcher and Rohrbaugh derived the intensity distribution formula based on Kirchhoff's principle, which is as follows:

$$I^2\left\{\frac{(\lambda+\mu c)^2}{(\mu-c\lambda)^2}\sin^2\frac{\pi u(\mu-c\lambda)}{l}+\frac{(\lambda-\mu c')^2}{(\mu+c'\lambda)^2}\sin^2\frac{\pi(a-u)(\mu+c'\lambda)}{l}\right.$$
$$\left.+2\frac{(\lambda+\mu c)(\lambda-\mu c')}{(\mu-c\lambda)(\mu+c'\lambda)}\sin\frac{\pi u(\mu-c\lambda)}{l}\sin\frac{\pi(a-u)(\mu+c'\lambda)}{l}\cos\frac{\pi a\mu}{l}\right\} \qquad \cdots\cdots(7)$$

In the same way as performed on Rowland's formula, (7) is reduced to a simple form

$$I^2\left[\sin\frac{\pi u(\mu-c\lambda)}{l}\right]^2\left[\frac{\lambda+c\mu}{\mu-c\lambda}-\frac{\lambda-c'\mu}{\mu-c'\lambda}\right]^2=I^2\left[\sin\frac{\pi u(\mu-c\lambda)}{l}\right]^2\left[\frac{(\mu^2+\lambda^2)(c+c')}{(\mu-c\lambda)(\mu+c'\lambda)}\right]^2$$
$$\cdots\cdots(8)$$

In the blazed directions, this becomes

$$\pi^2u^2(\lambda+\mu c)^2=\pi^2u^2\lambda^2(1+c^2)^2 \qquad \text{for} \quad \mu=c\lambda \qquad \cdots\cdots(9)$$

$$\pi^2(a-u)^2(\lambda-\mu c')^2=\pi^2(a-u)^2\lambda^2(1+c'^2)^2 \qquad \text{for} \quad \mu=-c'\lambda \qquad \cdots\cdots(10)$$

As the ratio of Rowland's formula (4) and Kirchhoff's formula (8), we obtain

$$\left[\frac{\frac{\sqrt{1+c^2}}{\mu-c\lambda}-\frac{\sqrt{1+c'^2}}{\mu+c'\lambda}}{\frac{(\mu^2+\lambda^2)(c+c')}{(\mu-c\lambda)(\mu+c'\lambda)}}\right]^2=\frac{(1+c^2)(1+c'^2)}{(c+c')^2}\sin\frac{\chi+\chi'}{2}\left[\frac{\cos\left(\frac{\phi+\psi}{2}+\frac{\chi'-\chi}{2}\right)}{\cos\frac{\phi-\psi}{2}}\right]^2 \quad \cdots\cdots(11)$$

where $\tan\chi=c$, $\tan\chi'=c'$.

The ratio (11) shows that in the case of $c=c'$ and normal incidence, (4) and (8) give the same intensity distribution and in other cases more or less different distributions.

IV. Numerical Calculations on Several Examples

Recalculations were carried out using several types of triangular grooves, which had been treated by Stamm and Whalen. In the case of symmetrical or nearly symmetrical grooves, the results obtained by Stamm and Whalen are considerably different from the results obtained using (4) and (8). In the cases of extremely unsymmetrical grooves, the diffracted light from wider side of the groove mainly contributes to the energy distribution and this means mathematically that the third term in (4) and (8) are very small and so is fortunately the miscalculated third term of (1). Hence in such cases (1) and (4) give nearly the same results. As the following numerical calculations show, (4) and (8) always give nearly the same results.

Case 1 Symmetrical grooves; $c=c'=0.14410$; $a=16966$A; $\angle A=\angle C=8°12'$; $\angle B=163°36'$; blazed at 4780A, first order; normal incidence:

Table I.

N	3	2	1	0	−1	−2	−3
ϕ	57°52′	34°22′	16°24′	0°	−16°24′	−34°22′	−57°52′
R K	0.04%	3.69%	26.04%	40.45%	26.04%	3.69%	0.04%
S	0.24%	15.10%	29.04%	11.24%	29.04%	15.10%	0.24%

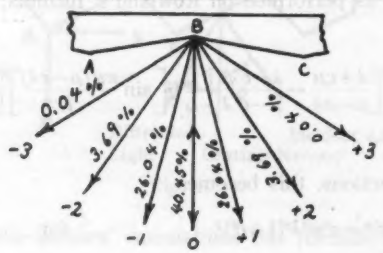

Fig. 2.

The energy distribution for l=4780A is given in Table I and Fig. 2. In the Table K, R and S stand for formulae (8), (4) and (1).

Case 2 Unsymmetrical grooves; c=0.27327; c'=0.14410; a=16933A; $\angle$A =15°17′; $\angle$B=148°19′; $\angle$C=8°12′; blazed at 4780A, first order; normal incidence:

The distribution for l=4780A is given in Table II and Fig. 3. Comparing Table II with Table I, it is revealed that the two gratings, which have the same grating constant and the same blazing wavelength, give different energy distribution due to the difference of the groove form.

Table II.

N	3	2	1	0	−1	−2	−3
ϕ	57°52′	34°22′	16°24′	0°	−16°24′	−34°22′	−57°52′
K	1.76%	11.02%	20.20%	18.91%	44.15%	3.35%	0.58%
R	1.81%	11.08%	19.82%	18.23%	45.43%	3.10%	0.52%
S	9.73%	15.80%	12.81%	10.20%	37.26%	9.37%	4.82%

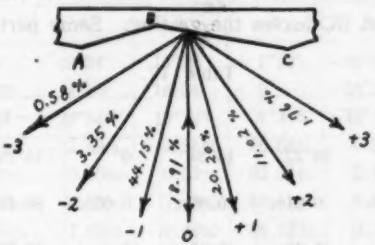

Fig. 3.

Case 3 Unsymmetrical grooves; c=0.58676; c'=0.30923; a=16933A; $\angle$A =30°24′; $\angle$B=132°25′; $\angle$C=17°11′; blazed at 4780A, second order; normal incidence:

Table III.

N	3	2	1	0	−1	−2	−3
ϕ	57°52′	34°22′	16°24′	0°	−16°24′	−34°22′	−57°52′
K	17.50%	7.89%	0.21%	6.50%	7.95%	59.12%	0.83%
R	20.15%	8.60%	0.22%	6.61%	7.82%	55.87%	0.74%
S	22.20%	4.31%	0.18%	2.42%	6.07%	63.50%	1.30%

The distribution for $l=4780$A is given in Table III and Fig. 4. In the cases 2 and 3 the values of u is chosen to about $a/3$.

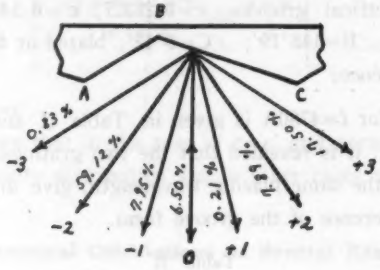

Fig. 4.

Case 4 Unsymmetrical grooves; $c=6.9393$; $c'=0.14410$; $a=16933$A; $\angle$A $=81°48'$; $\angle$B$=90°$; $\angle$C$=8°12'$; blazed at 4780A, first order; normal incidence:

The distribution for $l=4780$A is given in Table IV and Fig. 5. Differing from the above example, in this case the area of one side is very small compared with the other. Most of the light which is incident on AB diffracts toward BC and after diffraction at BC leaves the grating. Some part of the light which is

Table IV.

N	3	2	1	0	−1	−2	−3
ϕ	57°52′	34°22′	16°24′	0°	−16°24′	−34°22′	−57°52′
K	0.57%	0.21%	0.05%	0.00%	98.48%	0.18%	0.51%
R	1.42%	0.40%	0.07%	0.00%	97.75%	0.14%	0.22%
S	0.63%	0.29%	0.06%	0.03%	97.99%	0.19%	0.80%

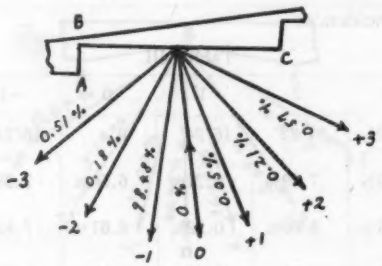

Fig. 5.

directly diffracted at BC also diffracts toward AC and diffracts once more. But as the area of AB is small, it will cause only slight errors. In the calculation, these effects are neglected. Table IV shows that when the area of one side is very small, formulae (4) and (1) give similar distributions.

Case 5 Unsymmetrical grooves; $c=0.30928$; $c'=3.2311$; $a=16933$A; $\angle A=17°11'$; $\angle B=72°49'$; $C=90°$; blazed at 4780A, second order; fixed angle mounting:

Fixing the angle between the collimator and the telescope so that the second order spectral line of 4780A diffracts to the direction of the grating normal, the grating was rotated to bring 4358A, 4780A, 5200A on the centre of the telescope. With this mounting $\phi=32°49'$, $34°22'$ and $35°56'$ for l=4358A, 4780A and 5200A, respectively. The intensity distributions are shown in Table V and Fig. 6 (Figure 6 shows only the case of 4780A). Hereafter only the formula (8) is used in calculation because, as the above cases show, (4) and (8) give always similar results and it has no meaning to calculate using both formulae. In the cases 4 and 5, formulae (8) and (1) give similar results. As pointed out by Stamm and Whalen,

Table V.

N		5	4	3	2	1	0	−1
ϕ	4358A	48°9′	29°34′	13°18′	− 1°33′	−16°32′	−32°49′	−53°4′
	4780A	57°52′	34°22′	16°24′	0°	−16°24′	−34°22′	−57°52′
	5200A	71°33′	39°54′	19°32′	1°34′	−16°15′	−35°56′	−63°23′
K	4358A	0.12%	1.59%	9.58%	86.68%	0.29%	0.55%	1.19%
	4780A	0.60%	0.00%	0.03%	92.95%	2.27%	2.94%	0.93%
	5200A	1.13%	0.83%	1.23%	83.52%	9.95%	3.27%	0.06%
S	4358A	0.34%	1.65%	9.49%	86.15%	0.28%	0.80%	1.50%
	4780A	0.48%	0.00%	0.19%	92.26%	1.73%	3.41%	1.88%
	5200A	1.67%	0.68%	1.00%	82.26%	10.93%	3.27%	0.19%

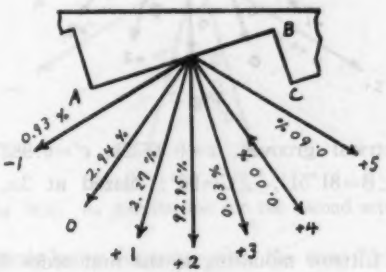

Fig. 6.

in this mounting, intensity falls away more rapidly on the high wavelength side of the blaze.

Case 6 Unsymmetrical grooves; $c=0.29426$, $c'=3.3977$; $a=16933$A; $\angle A=16°24'$; $\angle B=79°36'$; $\angle C=90°$; blazed at 4780A, second order; Littrow mounting:

In the Littrow mounting, $\phi=14°55'$, $16°24'$ and $17°53'$ for $l=4358$A, 4780A and 5200A, respectively. The intensity distributions for the three wavelengths, each with the above angle of incidence, are given in Table VI and Fig. 7 (Fig. 7 shows only for the wavelength 4780A). In the blazed direction the intensity concentrates more effectively than in the fixed angle mounting.

Table VI.

N		4	3	2	1	0	−1	−2
ϕ	4358A	51°5′	30°59′	14°55′	0°	−14°55′	−30°59′	−50°32′
	4780A	57°52′	34°22′	16°24′	0°	−16°24′	−34°22′	−57°52′
	5200A	67°7′	37°53′	17°53′	0°	−17°53′	−57°53′	−67°7′
K	4358A	0.00%	3.41%	93.69%	1.66%	0.03%	0.32%	0.89%
	4780A	0.97%	0.21%	93.60%	0.17%	0.06%	1.18%	0.52%
	5200A	1.66%	2.88%	85.93%	5.38%	2.54%	1.60%	0.01%
S	4358A	0.00%	3.15%	92.82%	1.78%	0.04%	0.44%	1.77%
	4780A	1.39%	0.23%	94.64%	0.25%	1.04%	1.50%	0.95%
	5200A	2.64%	2.72%	85.08%	5.40%	2.95%	1.19%	0.00%

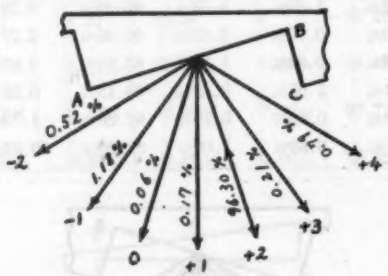

Fig. 7.

Case 7(a) Unsymmetrical grooves; $c=0.14321$, $c'=6.9827$; $a=10.5835\mu$; $\angle A=8°9'$; $\angle B=81°51'$; $\angle C=90°$; blazed at 3μ, first order; Littrow mounting:

When set for the Littrow mounting to the first order 3μ and the first order 6μ, $\phi=8°9'$ and $16°28'$, respectively. The 3μ distribution for the first setting

and the 3μ and 6μ distributions for the second setting are given in Table VII(a) and Fig. 8(a).

Table VII(a).

N		4	3	2	1	0	−1	−2	−3
ϕ	3*	82°47′	45°7′	25°10′	8°9′	− 8°9′	−25°10′	−45°8′	−82°49′
	3†	58°17′	34°32′	16°28′	0°	−16°28′	−34°32′	−58°17′	
	6†			58°17′	16°28′	−16°28′	−58°17′		
K	3*	0.73%	0.22%	0.04%	97.55%	0.04%	0.17%	0.44%	0.81%
S	3*	2.53%	0.30%	0.06%	94.01%	0.08%	0.39%	1.26%	1.37%
K	3†	0.34%	0.08%	0.01%	98.07%	0.26%	0.46%	0.77%	
S	3†	0.32%	0.06%	0.01%	97.63%	0.32%	0.65%	1.02%	
K	6†			4.66%	44.90%	46.42%	4.02%		
S	6†			4.98%	43.84%	42.92%	8.25%		

* First setting.
† Second setting.

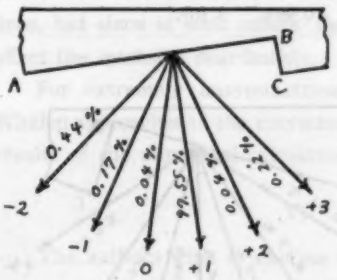

Fig. 8(a).
3μ distribution for the first setting.

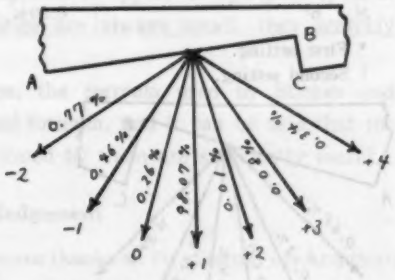

Fig. 8(a).
3μ distribution for the second setting.

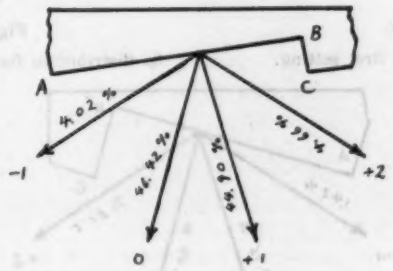

Fig. 8(a). 6μ distribution for the second setting.

Case 7(b) All constants being the same with the case 7(a) except $c=0.29558$, the grating is blazed to the first order of 6μ.

The distributions for the same setting with the case 7(a) are shown in Table VII(b) and Fig. 8(b). In the cases 7(a) and 7(b) formulae (8) and (1) give similar results, so Stamm and Whalen are still right in saying that when working through an octave, without changing orders and without a fore prism, it is best to blaze at (or below) the lower wavelength limit of the region under considerations.

Table VII(b).

N		4	3	2	1	0	−1	−2	−3
ϕ	3*	82°47′	45°7′	25°10′	8°9′	− 8°9′	−25°10′	−45°8′	−82°49′
	3†	58°17′	34°22′	16°28′	0°	−16°28′	−34°32′	−58°17′	
	6†			58°17′	16°28′	−16°28′	−58°17′		
K	3*	0.78%	2.05%	96.24%	0.04%	0.01%	0.23%	0.65%	0.00%
S	3*	2.23%	1.11%	94.23%	0.05%	0.35%	0.82%	0.59%	0.62%
K	3†	1.57%	0.73%	96.24%	0.00%	0.15%	0.59%	0.72%	
S	3†	1.14%	0.18%	95.86%	0.20%	0.84%	1.03%	0.75%	
K	6†			2.18%	96.24%	0.16%	1.42%		
S	6†			0.99%	94.93%	0.98%	3.10%		

* First setting.
† Second setting.

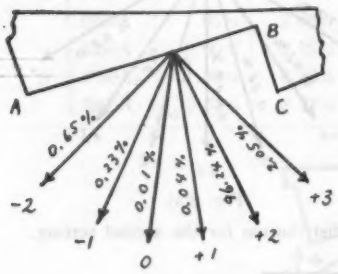

Fig. 8(b).
3μ distribution for the first setting.

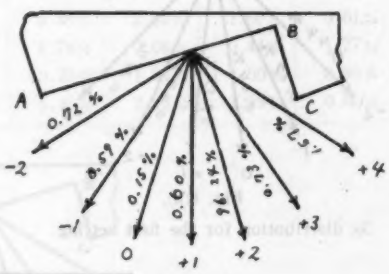

Fig. 8(b).
3μ distribution for the second setting.

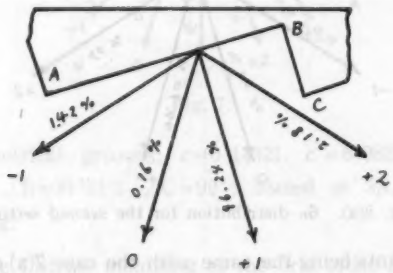

Fig. 8(b). 6μ distribution for the second setting.

V. Conclusion

Corrected formulae for energy distribution of diffracted light from plane gratings based on Rowland's method and on Kirchhoff's principle are derived, and numerical calculations on several examples were carried out. The formulae are derived on the assumption that the incident light reaches all parts of the groove surface and all the diffracted light contribute directly (no secondary reflection) to the intensities of every order. Although in real gratings this assumption is not perfectly fulfilled, the difference can be considered very small, the effect of multiple diffraction is therefore neglected in the numerical calculations. Corrected Rowland's formula and the formula used by Stamm and Whalen give considerably different results in the cases of symmetrical or nearly symmetrical grooves such as the cases (1) and (2) but in the case of extremely asymmetrical grooves, both formulae give similar results. The formula based on Kirchhoff's principle and that on Rowland's method give always nearly the same results. The effects of the inclination factor are expected to appear in high order spectral lines, but since in such orders the intensities are always small, they scarcely affect the intensity distribution.

For extremely unsymmetrical grooves, the formula used by Stamm and Whalen approaches to the corrected Rowland formula, and it can be said that the results of the numerical calculations performed by them are sufficiently useful.

VI. Acknowledgement

The authors wish to express their sincere thanks to Dr. Stamm of American Cyanamide Company for his kind suggestion concerning to this problem.

An Apparatus for Detecting Stains on Glass Surface and Determination of Refractive Index of the Stain

Kazuo MIYAKE

Institute for Optical Research, Tokyo University of Education

(Received November 15, 1956)

Abstract

A sensitive apparatus has been constructed for detecting stains on glass surface by illuminating it with linearly polarized light and observing the reflection at polarizing angle of the glass surface. Tests have been successful.

Refractive index of stain can be determined by measuring polarizing angle of the stain surface which was found to be 1.47 ± 0.01 for glasses F2 and SF3.

1. Introduction

Some kinds of glass are liable to be stained by inadequate treatments or even by being exposed to wet atmosphere. The stain is considered as due to an anomalous layer formed on the glass surface.

If this anomalous layer is considerably thick, it will be observed by its interference color, whereas a very thin layer is hardly observable to the naked eye. However, if it is coated with a reflection-reducing film, detection is made with ease even to the thickness of 5 mμ by a change of color.

Hence it is very desirable to find an effective method to detect the presence of such stain before the anti-reflection treatment. According to the principle, suggested by Y. Doi[1], an apparatus was constructed for this purpose, and refractive index of the anomalous layer was measured by using polarized light.

2. Apparatus for Detection

The light, reflected at polarizing angle from a surface of such dielectric substance as glass, consists exclusively of a component vibrating normally to incident plane. Therefore, no p-component vibrating parallel to the incident plane can be reflected.

If there is an anomalous layer on some part of the glass surface and linearly polarized light, consisting only of p-component, is thrown to the surface at polarizing angle, the reflection will come only from the anomalous layer revealing

1) Y. Doi: J. Appl. Phys. Japan **25** (1956) 469.

its presence.

According to this principle, an apparatus described below, was constructed with the purpose to facilitate observing and photographing the stains formed on plane glass surfaces.

Fig. 1 shows the schematic arrangement and Fig. 2 is a photograph of the apparatus.

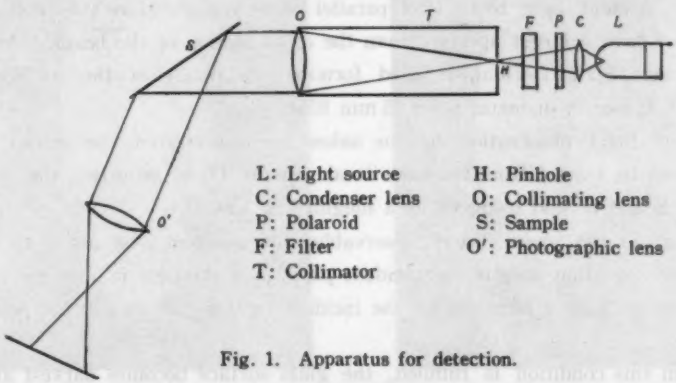

Fig. 1. Apparatus for detection.

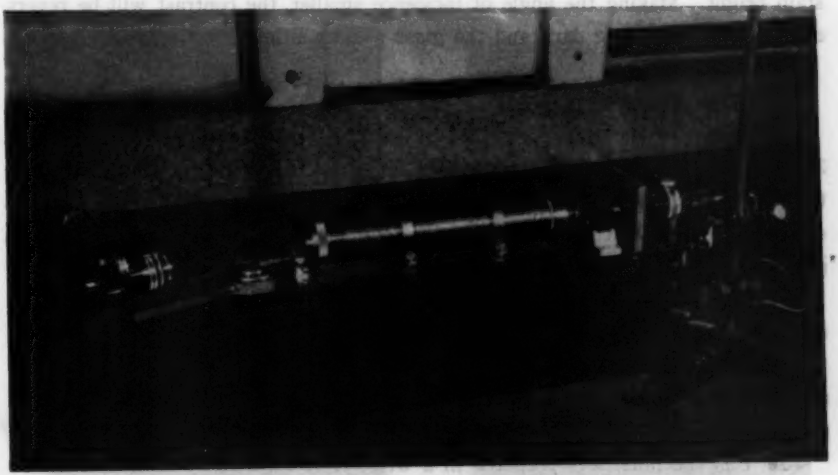

Fig. 2. Photograph of apparatus.

In Fig. 1 L represents a light source. A zirconium lamp was used. C represents a condenser lens, projecting the image of L onto a pinhole H of a collimator T. The pinhole has a circular aperture of 2 mm in diameter and the focal length of the collimating lens is 30 cm. F is a filter, which was used

when necessary. P is a polaroid, which can be rotated about the optical axis of the collimator T. The pinhole H is located at the focal point of the collimator lens O and therefore the light emerging from O becomes a parallel beam. S represents a turn table which supports a sample having stains on its surface and is made adjustable for the light to be incident at polarizing angle. O′ is a photographic lens projecting the surface under test onto a photographic film.

The incident light to O′ is of parallel beam and therefore the photographic lens must have a larger aperture than the cross section of the beam. A photographic lens, F/1.5, f=5 cm, is used forming the image of the surface to be tested of 32 mm in diameter upon 35 mm film.

When direct observation by the naked eye is preferred, the surface under test should be viewed from the back focal point of O′ by adjusting the distance between S and O′ and using O′ as a magnifying lens.

To make the stain clearly observable, the polaroid is so set as to let the component vibrating only in the incident plane pass through it and the inclination of the surface is adjusted for the incident light to fall on it at the polarizing angle.

When this condition is fulfilled, the glass surface becomes darkest and the stain bright. Making the angle of incidence smaller, the contrast will be reversed, the stain becoming dark and the glass surface bright.

3. Examples of Test

A series of photographs obtained by using this apparatus, are shown in Fig. 3. The glass tested was F2. A half of the surface of the specimen was protected by pitch and the exposed half was etched by dipping it in a 1N. aqueous solution of HNO_3 at 63–64°C for the length of time indicated under each photograph.

Among these specimens, the one etched by HNO_3 for 2 min. was so faintly stained that the stain was hardly detected by the naked eye.

In Fig. 4, the photograph shows the stain, which is called "water-stain" and was formed on the surface of SF3 glass immeadiately after the end of polishing.

As this specimen was prepared in a wedge form, the reflected light from the back surface was completely eliminated and the stain was observed with especially high contrast.

4. Determination of Refractive Index

As described above, the contrast can be reversed by making the angle of

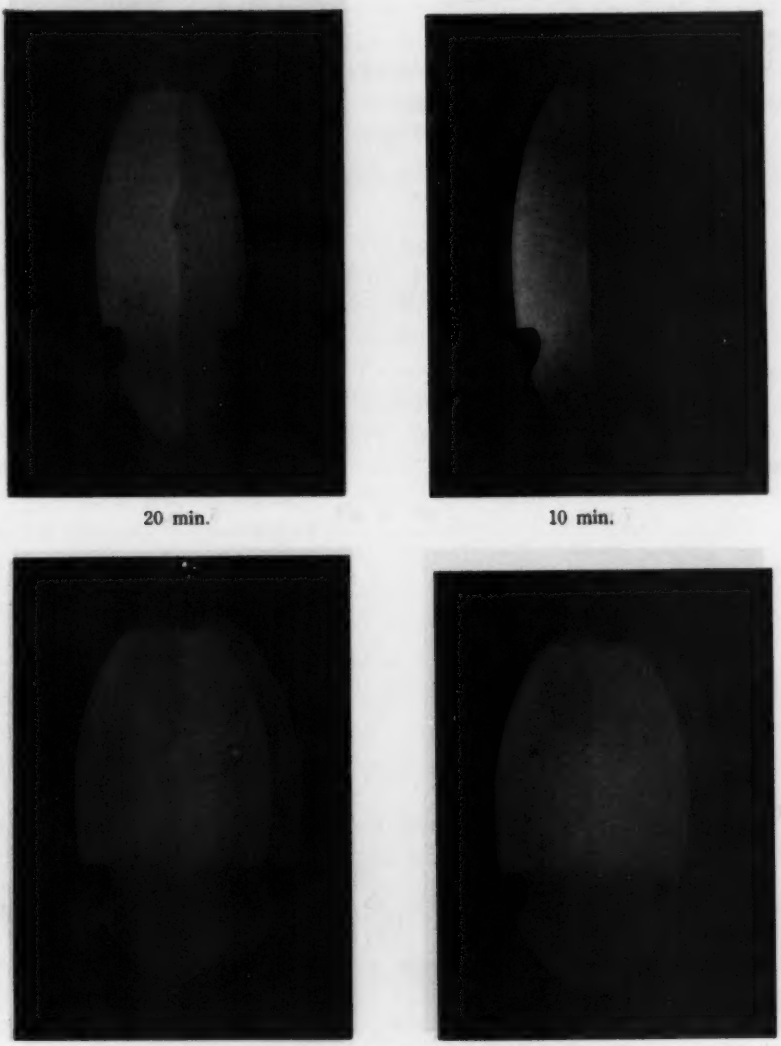

20 min. 10 min.

Fig. 3. (1)

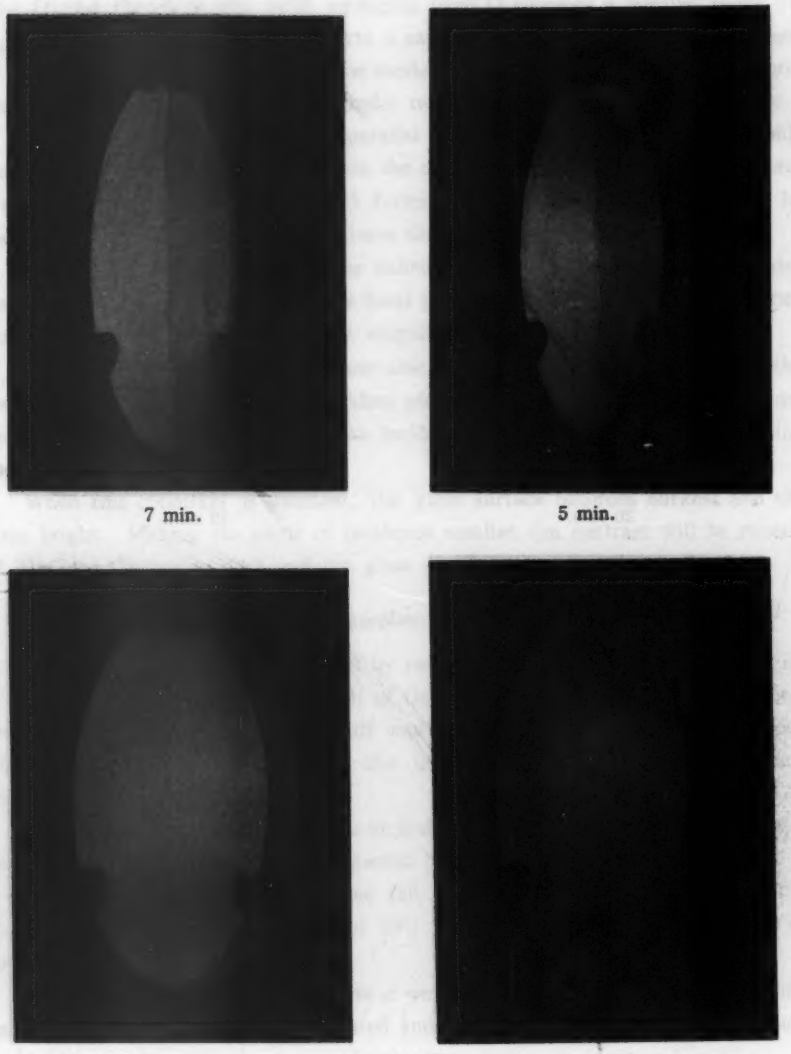

7 min. 5 min.

Fig. 3. (2)

2 min.

In Fig. 3 (1), (2), (3).
Upper side:
At polarizing angle of glass.
Lower side:
Contrast Reversed.

Fig. 3. (3)

At polarizing angle of glass

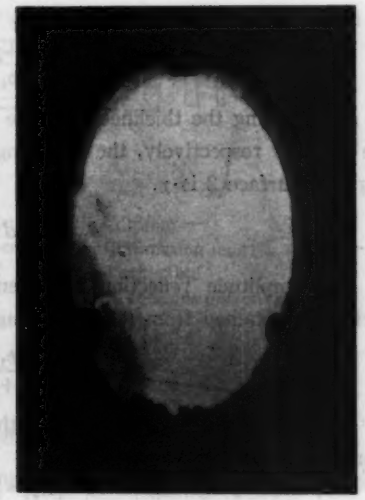

Contrast reversed

Fig. 4. "Water-strain" of SF3.

incidence small. Before the reversal, a position will be obtained, where the contrast disappears. This position can be found very precisely, because it is determined by comparing the brightness of the adjoining halves in the same field of view.

According to Abelés[2], the refractive index of surface layers can be determined by the measurement of the incident angle at this position.

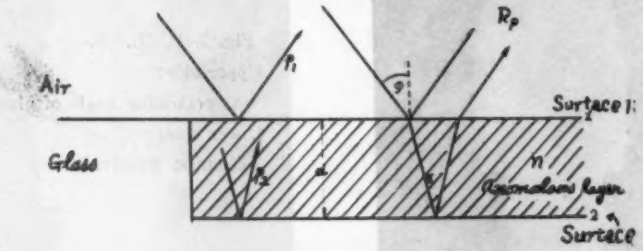

Fig. 5. Structure of stain.

Assume that a stain formed on a glass surface has a structure shown in Fig. 5 and the anomalous layers is homogeneous. Let the Fresnel amplitude reflection coefficient of p-component at Surface 1 be p_1, and that of Surface 2 be p_2. The amplitude reflection coefficient R_p for p-component of the stain is given as follows;

$$R_p=\frac{p_1+p_2e^{i\delta_p}}{1+p_1p_2e^{i\delta_p}} . \qquad \cdots\cdots(1)$$

If assuming the thickness and the refractive index of the anomalous layer are d and n respectively, the wavelength of light in vacuum is λ and the incident angle at Surface 2 is χ,

$$\delta_p=\frac{4\pi}{\lambda}nd\cos\chi \qquad \cdots\cdots(2)$$

The amplitude reflection coefficient R_{p0} of the p-component for the glass surface is obtained from (1) by putting δ_p in it equal to zero. That is,

$$R_{p0}=\frac{p_1+p_2}{1+p_1p_2} . \qquad \cdots\cdots(3)$$

If the reflection coefficients of the glass surface and the stain are equal, then

$$|R_p|=|R_{p0}| . \qquad \cdots\cdots(4)$$

This condition is fulfilled only in the case when

$$p_1=0 \quad \text{or} \quad p_2=0 . \qquad \cdots\cdots(5)$$

2) F. Abelés: J. Phys. et Rad. **11** (1950) 366.

Since $p_2=0$ occurs only in a special case when the refractive index of the anomalous layer is very low, it should be $p_1=0$, that is, the light is thrown onto the upper surface of the stain at the polarizing angle of the anomalous layer.

Measuring the incident angle at this position and using the formula $\tan\varphi=n$, the refractive index of the anomalous layer can be determined.

5. Measurement

According to Abelés' method described above, the refractive index of stain was measured.

The apparatus used was a common spectrometer and it was arranged as shown in Fig. 6. A super high pressure mercury lamp with a Wratten 77A filter was used as a light source, and the measurements were made for the green light of Hg λ 5461. A pinhole of 1 mm in diameter was placed at the focal point of a collimating lens of 210 mm focal length and the parallel beam emerging from the collimator was thrown upon the surface of specimen nearly at the polarizing angle of glass.

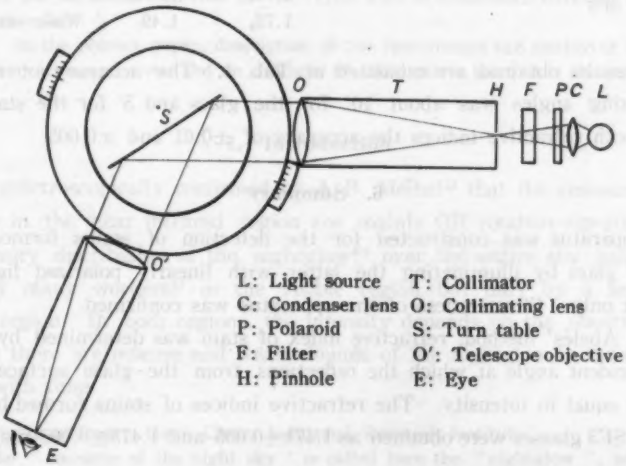

Fig. 6. Arrangement for measurement.

A polaroid was rotated until only p-component falls upon the surface. After the adjustment had been completed, the eyepiece of the telescope was replaced by a cap having a pinhole of 2 mm in diameter.

Rotating the turn table S holding the specimen and the telescope, two positions were determined, one where the contrast disappears and the other where

the contrast becomes highest.

Using the Brewster's formula

$$\tan\varphi = n, \qquad \ldots\ldots(6)$$

the refractive indices of the glass and the stain were calculated. The specimens measured were F2 glass plates, etched as before. SF3 glass plate etched for 1 min. in 1N. HNO_3 at 62°C and the same glass with "water-stain" were also measured.

Table I.

Glass	Time of etching (min)	Refractive index of glass	Refractive index of stain	Note
F2	20	1.61	1.47_8	Mean value glass: 1.62_5 stain: 1.47_1
	10	1.62	1.47	
	7	1.63_8	1.47_0	
	5	1.63	1.47_0	
	2	1.62_8	1.46_9	
SF3	1	1.74_0	1.47_8	
	—	1.73_5	1.49_3	Water-stain

The results obtained are tabulated in Tab. 1. The accuracy of measuring the polarizing angles was about 10′ for the glass and 5′ for the stain, which give for both refractive indices the accuracy of ± 0.01 and ± 0.005.

6. Summary

An apparatus was constructed for the detection of stains formed on the surface of glass by illuminating the latter with linearly polarized light of *p*-component only. Effectiveness of the apparatus was confirmed.

Using Abelés' method, refractive index of stain was determined by measuring the incident angle at which the reflections from the glass surface and the stain were equal in intensity. The refractive indices of stains formed by etching on F2 and SF3 glasses were obtained as 1.471 ± 0.005 and 1.475 ± 0.005 respectively.

7. Acknowledgement

The author wishes to express his thanks to Mr. Y. Doi of the Government Mechanical Laboratory, who gave him valuable advice.

He is also obliged to the Ministry of International Trade and Industry and the Camera Research Association of Japan, for supporting him with the expense of this work.

Photoelectric Studies of Near Infrared OH Emissions of the Night Sky (I)

Masaru OGAWA, Masatoshi, NAKAMURA and Akio HASHIZUME*

Institute for Optical Research, Tokyo University of Education

(Received October 8, 1956)

Abstract

A set of photometer for surveying the near infrared OH emission of the night sky has been made. This is a preparation for the coming International Geophysical Year. The method of photometry adopted is as follows.

1. For the detector, an Ag-Cesium photoelectric tube is used.
2. In order to eliminate the zero drift which appears in direct dark current of photoelectric tube, an a. c. amplification is adopted.
3. A synchronous rectifier is used to reduce the noise which appears in the output of amplifier.

With the above arrangement, the intensity distribution of the emission and its variation with time are surveyed with an altazimuth covering the entire sky.

In the present paper, description of the instruments and method of the observation are given and an example of photometric records is shown.

1. Introduction

It is spectroscopically confirmed by A. B. Meinel[1] that the emissions of the night sky in the near infrared region are mainly OH rotation-vibration bands. The intensity distribution of the nightglow** over the entire sky has been observed by many workers[2] in the visible region but only by a few[3] in the infrared region. In both regions, the intensity depends on the observer's local time, and there are intense and weak clounds of the nightglow in the entire sky, drifting with time.

* Present address; Govt. Chem. Industrial Research Institute.

** The "emission of the night sky" is called here the "nightglow", according to F. E. Roach.

1) A. B. Meinel: Ap. J., **111**, (1950) 555.

2) For example, F. E. Roach and H. B. Pettit: Jour. Geophys. Res., **56** (1951) 325, and M. Huruhata, H. Tanabe and T. Nakamura: Report of Ionosphere Research in Japan, **IX**, No. 3, (1955) 136.

3) M. Huruhata: Report of Ionosphere Research in Japan; **IV** No. 3, (1950) 137, **VI**, No. 1, (1952) 31. Kron: P.A.S.P., **62**, (1950) 264.

As regards the height of the emitting layer, the cause of drift of the clouds and the mechanism of the nightglow, there is much to be learnt.

The purpose of the present work is to form a link in the chain of observations during the International Geophysical Year beginning in July 1957 by making observations on the intensity distribution of near infrared OH emission over the entire sky and obtaining informations as to the height of the emitting layer, drift of the clouds and other outstanding problems closely in concert with the observation group of the nightglow under the leadership of Dr. M. Huruhata of Tokyo Astronomical Observatory.

2. Instruments and Results

As shown in Fig. 1, the measuring arrangement consists of the following parts:

(A) Reflection altazimuth with optical equipment. Setting of azimuth and altitude is made automatic.

(B) 50 cycle oscillator for chopping motor.

(C) Detector and amplifier.

(D) Synchronous rectifier and recorder.

(E) Independent power supply for each of oscillator, amplifier and rectifier.

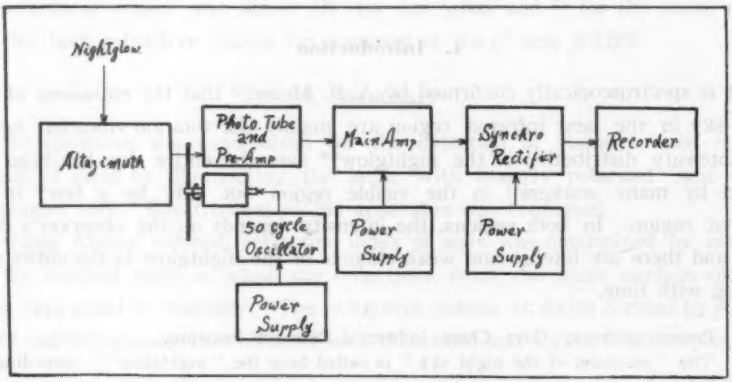

Fig. 1. Block diagram of the instruments.

(A) *Automatic Reflection Altazimuth*

The construction of the main part of the reflection altazimuth except some optical equipment is after the principle of Dr. Huruhata's design and shown in Fig. 2.

(M_1) is a plane mirror, the surface of which is coated with gold film, and is

fitted at an angle of 45° at the end of a horizontal shaft (*H*). The axis of which is in line with the axis of a lens (*L*) of 7 cm in aparture and 22 cm in focal length.

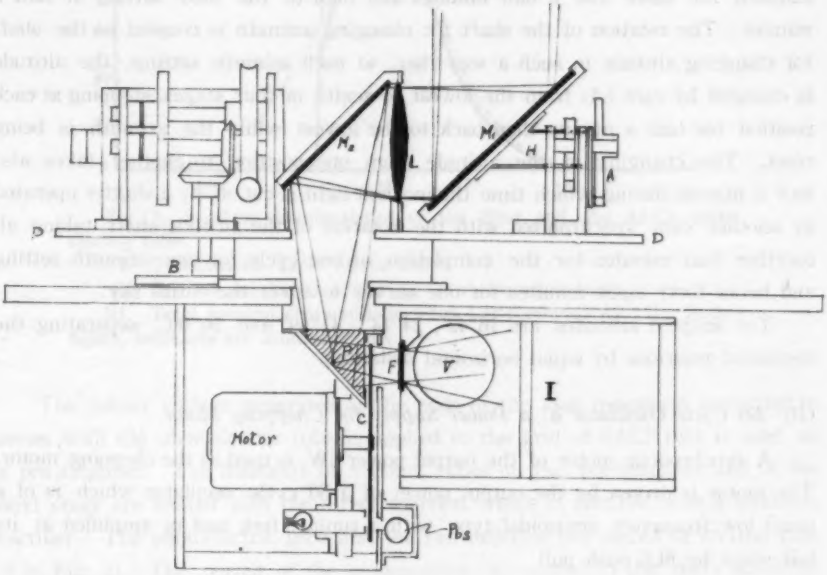

Fig. 2. Schematic diagram of the altazimuth.
A: Cam for changing altitude.
H: Shaft connected with cam (A).
M_1, M_2: Plane mirrors coated with gold film.
L: Lens of 7 cm in aparture and 22 cm in focal length.
P: Right angle prism.
C: Chopper.
F: Filter.
V: Ag-Cs photoelectric tube.
I: Enclosure with the photoelectric tube and pre-amplifier.
D: Brass plate.
B: Cam for changing azimuth.

The shaft (*H*) is rotated by a specially shaped cam (*A*) to admit the radiation from the sky at various altitudes into a photoelectric tube (*V*) through the lens (*L*), reflected by another gold coated plane mirror (M_2) and a right angle prism (*P*), chopped at 125 cycles by a chopper (*C*) and finally through a filter (*F*). The filter with its spectral transmission curve as shown in Fig. 3, fitted in the focal plane of the lens, is to eliminate the light from the stars and visible stray lights that disturb the measurement. A field stop in front of the filter enables the

measurement of the sky of a circular area of 5° in diameter.

A phonomotor operates the mounting above the brass plate (*D*) to change the azimuth setting into twelve different directions by cam (*B*), stopping at each azimuth for three and a half minutes and then to the next setting in half a minute. The rotation of the shaft for changing azimuth is coupled to the shaft for changing altitude in such a way that, at each azimuth setting, the altitude is changed by cam (*A*) from the lowest to zenith in four stages, stopping at each position for half a minute then back to the lowest while the azimuth is being reset. The changing of the altitude from one position to another takes also half a minute during which time the incident light is cut off by a shutter operated by another cam synchronized with the rotation of the altitude shaft taking altogether four minutes for the completion of one cycle for one azimuth setting and hence forty eight minutes for one survey to cover the entire sky.

The adopted altitudes are 16°42′, 24°14′, 41°59′ and 90°00′, separating the measured positions by equal horizontal distances.

(*B*) *50 Cycle Oscillator as a Power Supply for Chopping Motor*

A synchronous motor of the output power 2W, is used as the chopping motor. The motor is driven by the output power of a 50 cycle oscillator which is of a usual low frequency sinusoidal type with a tuning fork and is amplified at its last stage by 6L6 push pull.

(*C*) *Detector and Amplifier*

It is considered that both PbS photoconductive cell and Ag-Cesium photoelectric tube can be satisfactory as sensitive detectors for the wavelength range concerned.

In preliminary experiments, it was confirmed that a PbS photoconductive cell made by one of the authors can detect the nightglow. However, since there are strong absorptions of water vapor in the sensitive region of PbS cell and the amount of water vapor varies diurnally, Ag-Cesium photoelectric tube was finally adopted as the detector. The spectral sensitivity of the photoelectric tube is shown in arbitrary units in Fig. 3. In the figure, a curve with a bold real line is the total spectral characteristic when the photoelectric tube and the filter are used in combination. It is, therefore, considered that almost all of the radiation measured with this combined detector are the rotation-vibration bands of OH molecules. There is a double band at λ 8645, due to O_2 but it can be neglected in the measurement because its intensity is weak in comparison with that of OH bands, which extend over a wide range.

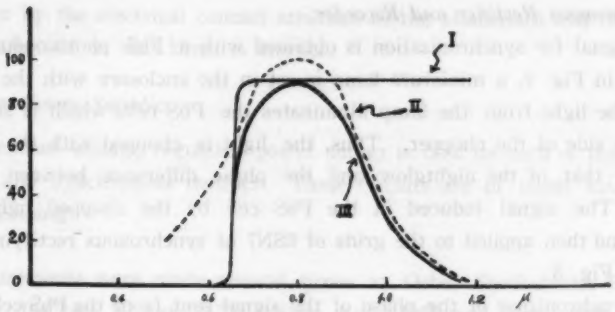

Fig. 3. Spectral characteristics of the filter and the Ag-Cs photoelectric tube.
I. Transmission curve of the filter.
II. Spectral sensitivity of the Ag-Cs photoelectric tube.
III. Total spectral characteristic when I is combined with II. In this figure, ordinates are arbitrary units.

The output voltage generated at the ends of the load resistance connected in series with the photoelectric tube is applied to the grid of 6AC7 that is used as a pre-amplifier. The filaments of vacuum tubes of the pre-amplifier and of the next stage are heated with the direct currrent which is rectified with a selenium rectifier. The photoelectric tube and the pre-amplifier are placed in an iron case (I in Fig. 2). The output of the pre-amplifier is applied to the main amplifier set in an observation shelter built about three meters away from the altazimuth.

The main amplifier is a narrow band amplifier with Twin-T circuit as shown in Fig. 4. The band width is 3~4 cycles. The amplified signal is applied to the input of the synchronous rectifier and rectified there.

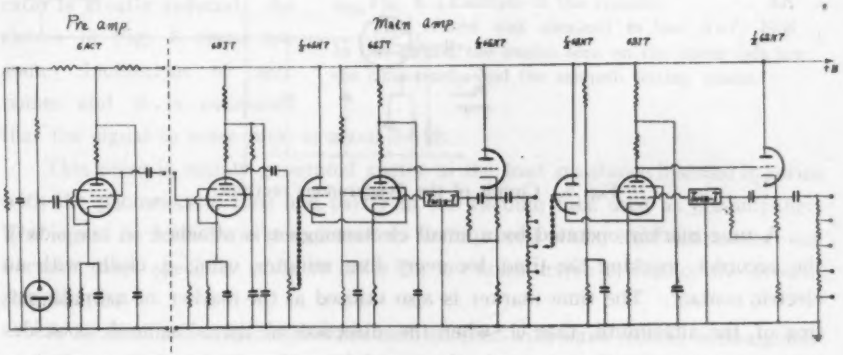

Fig. 4. Circuit of the amplifier.

(D) Synchronous Rectifier and Recorder

The signal for synchronization is obtained with a PbS photoconductive cell. As shown in Fig. 2, a miniature lamp is set in the enclosure with the chopping motor. The light from the lamp illuminates the PbS cell, which is situated at the oposite side of the chopper. Thus, the light is chopped with the same frequency as that of the nightglow and the phase difference between them are constant. The signal induced in the PbS cell by the chopped light is first amplified and then applied to the grids of 6SN7 of synchronous rectifying circuit, as seen in Fig. 5.

The synchronizing of the phase of the signal sent from the PbS cell and that of the output of the main amplifier is controlled by adjusting the variable resistance (S) inserted in the middle of the circuit shown at left side in Fig. 5. In this method of synchronizing, some changes in the wave form of the amplified signal are introduced. Although this effect is undesirable, it did not cause much trouble in the present work.

The rectified d. c. output is smoothed up with a filter circuit and supplied to the input of the recorder.

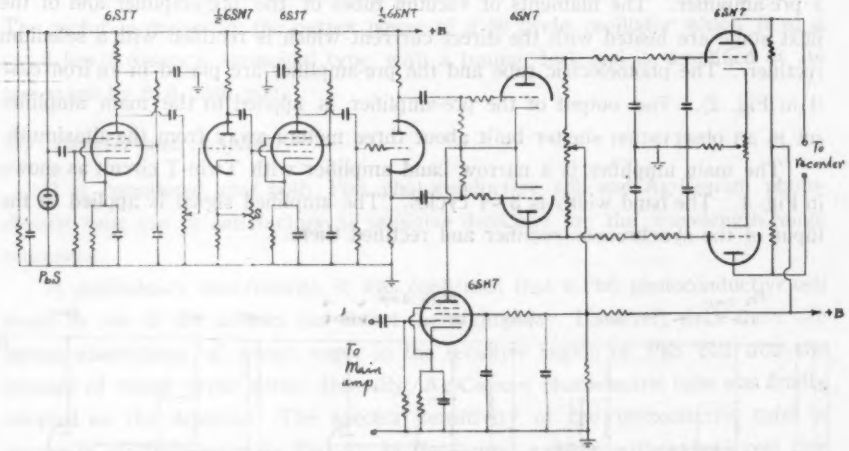

Fig. 5. Circuit of the Synchronous rectifier.

A time marker operated by a small electromagnet is attached on one side of the recorder marking the time for every five minutes using a clock with an electric contact. The time marker is also utilized as the marker of azimuth setting of the altazimuth, that is, when the direction of the altazimuth coincides with a certain azimuth, say north, the signal from the altazimuth is supplied to

the marker by the electrical contact attached to the altazimuth and the azimuth of the altazimuth, at that time, is marked.

(*E*) *Three Power Supplies*

Independent voltage regulated power supply is used for each of the oscillator, amplifier and synchronous rectifier. These circuits are of usual kind and not worth describing.

Measurements were made several times at Oobe, Shodoshima, Seto inland sea (Long. 134°16.5′ E, Lat. 34°32.7′N) in Aug. 1956 and Nov. 1956 using the above-mentioned instruments. An example of the records is shown in Fig. 6. In this figure, the regularly spaced marks seen on the upper side are the time marks for every five minutes and the irregular marks are the marks when the azimuth of the altazimuth was north at each time.

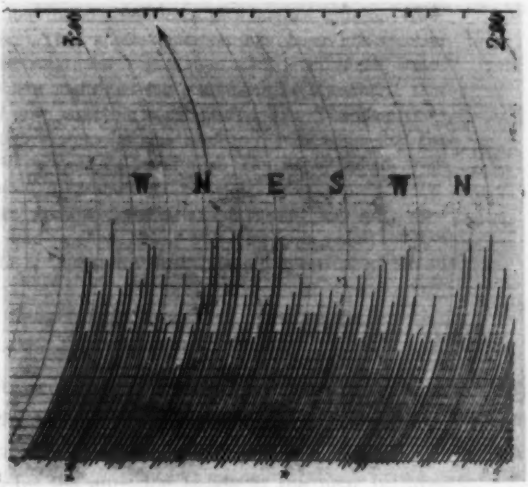

Fig. 6. Example of the records.
This record was obtained in Nov. 6~7, 1956. In this figure, the marks seen on the upper side are the time marks and the azimuth setting marks.

3. Conclusion

Under the present condition, since the noise due to the pre-amplifier is considerably large, signal to noise ratio is greatly reduced. As shown in Fig. 6, there are some fluctuations of zero points and it is estimated that the signal to noise ratio is about 8~20.

This noise is mainly generated partly in the load resistance inserted in series with the photoelectric tube and partly in the vacuum tube used as pre-amplifier. The signal to noise ratio is expected to be improved when load resistances and vacuum tubes specially made to order for low noise arrive to replace the present components.

A form of a.c. amplification has been adopted with some success in straightening the zero point drift due to direct dark current of photoelectric tube and in

increasing the stability and gain of the amplifier.

4. Acknowledgements

The authors wish to express their sincere thanks to Dr. Y. Fujioka and Dr. H. Ootuka for their deep interest and encouragement and to Dr. Huruhata of Tokyo Astronomical Observatory for his valuable suggestion and discussion.

Rotational Constants of B' State of Nitric Oxide and (Vibrational and Rotational Constants of $X^2\Pi_r$ and $B^2\Pi_r$)

Masaru OGAWA and Midori SHIMAUCHI

Institute for Optical Research, Tokyo University of Education

(Received October 15, 1956)

Abstract

Rotational analyses of $\beta'(3-0)$ band in the far ultraviolet absorption and $(0-0)$ and $(3-4)$ bands of $(B'-B)$ system in the near infrared emission are carried out using the low dispersed spectra in a method different from normal rotational analysis. This special method has been effective in obtaining a fairly accurate rotational constant of $v=3$ level of B' state, i. e. $B_3=1.263\pm0.002$, and has confirmed the conclusion of Miescher[1] that B' state is an inverted $^2\Delta$ with coupling constant $A\approx-2$. The identity of the upper state of these two systems is also confirmed indicating that the height of $v=4$ level of $B^2\Pi_r$ should be lower than can be expected from the position of levels of $v=0$, 1, 2 and 3.

In the Appendix there are listed the new vibrational and rotational constants of $B^2\Pi_r$, $X^2\Pi_r$ and $\nu_{0,0}$ of $B^2\Pi_r$, obtained as a result of the rearrangement of the data of β-system[3] and infrared spectroscopy[3),4)] of Nitric Oxide.

1. Introduction

Recent works in the spectroscopy of nitric oxide have revealed the existence of the B' electronic state, and its vibrational levels of $v'=0$, 1, 2 and 3 have been confirmed by the vibrational analyses of absorption[5),6),7)] and emission[8),9)] spectra in the far ultraviolet and also by the emission bands in the near infrared[10)].

Quite recently Miescher[1)] has obtained the rotational constants of vibrational levels of $v'=0$ and 1, as a result of the rotational analyses of four bands of β'

1) E. Miescher: Canad. J. Phys. **33** (1955) 355.
2) F. A. Jenkins, H. A. Barton and R. S. Mulliken: Phys. Rev. **30** (1927) 150.
3) R. H. Gillet and E. H. Eyster: Phys. Rev. **56** (1939) 1113.
4) N. L. Nichols, C. D. Hause and R. H. Nobel: J. Chem. Phys. **23** (1955) 57.
5) Y. Tanaka, M. Seya and K. Mori: Science of Light **1** (1951) 80, J. Chem. Phys. **19** (1951) 979.
6) L. H. Sutcliffe and A. D. Walsh: Proc. Phys. Soc. **A66** (1953) 209.
7) Miss M. Ueda: Science of Light **3** (1955) 143.
8) P. Bear and E. Miescher: Helv. Phys. Acta **24** (1951) 331.
9) Y. Tanaka: J. Chem. Phys. **21** (1953) 788.
10) M. Ogawa: Science of Light **2** (1953) 87.

system, namely 1633.5 A (1−0), 1739.3 A (1−2), 1775.9 A (0−2) and 1835.1 A (0−3) bands, and found that the upper state is an inverted $^2\Delta$ with coupling constant $A \approx -2$.

The authors have tried to make rotational analyses of the 1575 Å band of the far ultraviolet absorption and the 6898 Å and 7140 Å band of the near infrared emmission; these have been assigned to the (3−0) band of $\beta'(B'-X^2\Pi)$ system and the (0−0) and (3−4) bands of $(B'-B)$ system respectively. On photographs these bands are not sufficiently separated to make a normal rotational analysis. However, with the aid of accurately known rotational constants of the lower states of these systems the rotational constants of the upper states were able to be obtained from the observed wave numbers of the heads and slightly separated lines. The result of the analyses shows that this method is effective in obtaining a fairly accurate rotational constant from the spectrum of low dispersion and resolution. It has been confirmed that the upper states of these systems are the same and the rotational and coupling constants of this state are equal to that of B' state obtained by Miescher[1].

In order to perform this analysis the constants of $B^2\Pi_r$ state were examined following the original papers[3),11)]. Inspite of excellent accuracy in the measurement of the β-system by Jenkins, Barton and Mulliken[2], it has been found that the value of $\nu_{0,0}$ obtained by them as a result of the extrapolation of their empirical formula seems too high. Besides, the constants in their empirical formula are not simply related to those of recent spectroscopy. Making use of the result of recent works the observed values of Jenkins, Barton and Mulliken are rearranged in the general formula consisting of the notations of recent spectroscopy. The constants of $X^2\Pi_r$ and $B^2\Pi_r$ thus obtained are listed in the Appendix.

2. Rotational Analysis of $\beta'(3-0)$

The absorption spectrum of, $\beta'(3-0)$ band (1575 A), photographed with a 3-meter grazing incidence vacuum spectrograph was used for analysis. Its dispersion is not sufficient (2.5 A/mm) to separate the lines of the 12 possible branches. The lines clearly appearing are the result of the overlapping of several rotational lines in the region of $\pm 1\,cm^{-1}$. Since the rotational constants of the lower state are precisely known, the B' value most suitable to the measured wave numbers of the sharp heads and twenty rotational lines is obtained in the following way. Between cases a and b, the upper state is considered to be close to case b, so that the rotational terms can be expressed in the following formula of Hill-Van Vleck.

11) R. Schmid: Z. f. Physik **64** (1930) 84.

$$F_1(K)=B_v'[K(K+1)-A^2+Y(4-Y)/8(K+1)+\cdots];\ K=J-1/2$$
$$F_2(K)=B_v'[K(K+1)-A^2-Y(4-Y)/8(K+1)+\cdots];\ K=J+1/2 \qquad (1)$$
$$Y=A/B_v$$

Referring to the result of Miescher[1] the value $A=2$ and $A=-2$ are assumed here.

The third terms of these formulae can not be neglected for low J values for it strongly affects the position of the heads because of the minus sign of A and the value of $A^2=4$. The lower state can be regarded as near case a; therefore the rotational terms would be expressed in the following formulas.

$$F_1(J)=B_{0,1,\,\mathrm{eff}}[J(J+1)-\Omega^2];\ \Omega=1/2$$
$$F_2(J)=B_{0,2,\,\mathrm{eff}}[J(J+1)-\Omega^2];\ \Omega=3/2 \qquad (2)$$

The amount of Λ-type doubling of both states is possibly within the error of the present measurement. With these assumptions the following equations express the wave numbers of the possible 12 branches.

$$Q_{11}(J)=(\nu_0^{(1)}-4B'+B_1''/4)-B'/4+B'Y(4-Y)/2(J+1/2)-B_1''J+(B'-B_1'')J^2$$
$$P_{21}(J)=(\nu_0^{(1)}-4B'+B_1''/4)-B'/4-B'Y(4-Y)/2(J+1/2)-B_1''J+(B'-B_1'')J^2$$
$$R_{11}(J)=(\nu_0^{(1)}-4B'+B_1''/4)+3B'/4+B'Y(4-Y)/2(J+3/2)+(2B'-B_1'')J$$
$$+(B'-B_1'')J^2$$
$$Q_{21}(J)=(\nu_0^{(1)}-4B'+B_1''/4)+3B'/4-B'Y(4-Y)/2(J+3/2)+(2B'-B_1'')J$$
$$+(B'-B_1'')J^2$$
$$P_{11}(J)=(\nu_0^{(1)}-4B'+B_1''/4)+3B'/4+B'Y(4-Y)/2(J-1/2) \qquad (3)$$
$$-(2B'-B_1'')J+(B'-B_1'')J^2$$
$$R_{21}(J)=(\nu_0^{(1)}-4B'+B_1''/4)+15B'/4-B'Y(4-Y)/2(J+5/2)$$
$$-(4B'-B_1'')J+(B'-B_1'')J^2$$
$$Q_{12}(J)=(\nu_0^{(2)}-4B'+3B_2''/4)-B'/4+B'Y(4-Y)/2(J+1/2)$$
$$-B_2''J+(B'-B_2'')J^2$$
$$P_{22}(J)=(\nu_0^{(2)}-4B'+3B_2''/4)-B'/4-B'Y(4-Y)/2(J+1/2)$$
$$-B_2''J+(B'-B_2'')J^2$$

and so on.

$B_1''=B_{0,1,\mathrm{eff}}$ (for $X^2\Pi_{1/2}$) and $B_2''=B_{0,2,\mathrm{eff}}$ (for $X^2\Pi_{3/2}$) in the above equations are determined according to the measurement in the microwave[12,13] and infrared[3),4)] to be $B_1''=1.67197$ and $B_2''=1.7224$.

As for B' the value calculated by extrapolating the constants obtained by Miescher[1] is 1.2635, which was used at first to estimate the wave numbers of each line of twelve branches. And its Fortrat diagram was drawn, which showed

12) C. A. Burrus and Walter Gordy: Phys. Rev. **92** (1953) 1437.
13) J. J. Gallagher, F. D. Bedark and C. M. Thomson: Phys. Rev. **93** (1954) 729.

that the head of the shortest wave length is formed by the rotational lines of R_{21} branch between $J=3^1/_2$ and $4^1/_2$ and that it is possible for four lines of Q_{21}, R_{11}, P_{21} and Q_{11} branches beyond $J=6^1/_2$ are to appear as one line owing to the near coincidence of position. The relative positions of these lines and heads agree so well with those of the observed, that the numbering of J for each observed line can easily be assigned. It seems quite right to conjecture that the rotational constant of the upper state, B' in the equations (3), is near to 1.2635. Therefore, in order to find the best B' value to explain the observed values, the amount of B' in the equations (3) has been varied by 0.002 cm^{-1} over the region from 1.250 to 1.274 to calculate the wave number of each line of each branch. Using these calculated values ν_0s suitable to each observed head and line are obtained. When B' is assumed to be 1.250, the $\nu_0^{(1)\prime}=(\nu_0^{(1)}-4B'+B_1''/4)$ should increase as J increases (cf. Table 1), which shows this B' value is too small to

Table 1.

$\nu_0^{(1)}$ Suitable to each observed value, $B'=1.250$.

$\nu_{obs.}$	I.	P_{21}, $\nu_0^{(1)\prime}{}_{cal.}$	Q_{11}, $\nu_0^{(1)\prime}{}_{cal.}$	Q_{21}, $\nu_0^{(1)\prime}{}_{cal.}$	R_{11}, $\nu_0^{(1)\prime}{}_{cal.}$
		$J=6^1/_2$	$J=6^1/_2$	$J=9^1/_2$	$J=9^1/_2$
63444.4	3	63474.2	63472.6	63473.2	63474.2
		$J=7^1/_2$		$J=10^1/_2$	
36.8	3	74.1	72.7	74.1	75.1
29.5	4	75.2	73.9	74.4	75.3
20.0	5	74.8	74.7	74.3	75.1
		$J=10^1/_2$			
10.2	5	75.1	74.1	74.6	75.4
63399.5	5	74.9	74.0	74.5	75.2
87.9	5	75.5	74.6	75.2	75.9
76.3	5	76.5	76.2	77.7	77.8
63.3	6_d	77.0	76.2	76.8	77.4
		$J=15^1/_2$	$J=15^1/_2$	$J=18^1/_2$	$J=18^1/_2$
48.1	5	76.1	75.4	76.0	76.6

$\nu_0^{(1)\prime}=\nu_0-4B'+B_1''/4$.

explain the measured wave numbers. Conversely, when $B'=1.274$ is adopted $\nu_0^{(1)\prime}$ should decrease as J increases. Any change in assigning the number of J for observed lines makes it impossible to obtain common $\nu_0^{(1)\prime}$ for observed head and lines. Thus it was found that the amount of B' should lie between 1.257 and 1.270 to be able to find common $\nu_0^{(1)\prime}$ in the experimental error. For each B' in this region the most suitable ν_0 was determined by averaging the slightly different ν_0s. The sum of this ν_0 and the calculated rotational term value of each line of each branch was compared with the each observed value. In the case when B' is greater than 1.265 the four lines expected to nearly coincide

should scatter in the wider region of $\pm 1\,cm^{-1}$, which suggests the observed lines should be more diffuse. Furthermore calculated values have the tendency to become greater than the observed ones with the increase of J (cf. Table 2).

Table 2.
Comparison of observed with calculated values;
$B'=1.270$, $\nu_0^{(1)'}=63471.8$

$\nu_{obs.}$	I.	$\nu(Q_{21})_{cal.}$	$\nu(R_{11})_{cal.}$	$\nu(P_{21})_{cal.}$	$\nu(Q_{11})_{cal.}$
		$J=11^1/_2$	$J=11^1/_2$	$J=8\ ^1/_2$	
63429.5	4	63429.9	63429.0	63428.7	
					$J=9^1/_2$
20.0	5	21.1	20.3	19.8	63418.7
10.2	5	11.5	10.8	10.0	09.0
63399.5	5	01.1	00.4	63399.5	63398.5
87.9	5	63389.8	89.1	88.1	87.2
76.3	5	77.8	77.2	75.9	75.2
		$J=17^1/_2$			
63.3	6_d	65.1	64.5	63.3	62.6
48.1	5		50.7	49.5	48.8
			$J=19^1/_2$	$J=16^1/_2$	$J=16^1/_2$
33.8	4		36.4	34.7	34.0

Conversely when B' is less than 1.260, the calculated wave numbers become less than the observed ones for high J value. In this way the best B' value to explain the observed values has been determined to be $1.263\pm0.002\,cm^{-1}$ and in this case the band origins should be $\nu_{3,0}^{(1)}=63477.5\pm0.2$ and $\nu_{3,0}^{(2)}=63353.1\pm0.2\,cm^{-1}$. The amounts of $\nu_{3,0}^{(1)}$ and $\nu_{3,0}^{(2)}$ designated here means the wave numbers between the mid point of the rotationless state ($F(J)=0$, i. e. the height of $J=0$ and $\Omega=0$) of $B'\,^2\Delta_{5/2}$ and $B'\,^2\Delta_{3/2}$ and the rotationless states of $X^2\Pi_{1/2}$ and $X^2\Pi_{3/2}$ respectively. In Table 3 the observed values are compared with the calculated ones for each line of each branch. It can be recognized from this table that only the main branches such as R_{21}, P_{21} and Q_{21} appear when J is small and satellite branches such as Q_{11}, R_{11} and P_{11} become more intense for high J, which shows, as suggested by Miescher[1], the upper state approaches pure case b as J increases. Two sharp heads are formed in the R_{21} and R_{22} branches. The Q_{21} and Q_{22} branches which seem able to make heads in some cases do not form heads with this B' value. In the region separated from the head of $63485.0\,cm^{-1}$ about 10 cm^{-1}, it is so clouded by the rotational lines of Q_{21} and R_{11}, that it seems to be a diffuse head in the low dispersed spectrum.

Although this methods of rotational analysis is quite troublesome, it seems to be effective in obtaining fairly precise rotational constants from insufficiently

separated spectrum, when the rotational constant of one of the two states is accurately known and that of the other can be roughly estimated.

Table 3.

$\beta'(3-0)$ Comparison of observed with calculated values

$B'=1.263$ $\nu_{3,0}^{(1)}=63477.5$ $\nu_{3,0}^{(2)}=63353.1\,\mathrm{cm}^{-1}$

$\nu_{obs.}$	Int.	$\nu(Q_{21})_{cal.}$	$\nu(R_{11})_{cal.}$	$\nu(R_{21})_{cal.}$				
63485.0	6			$J=1^1/_2$ 63482.8,	$J=2^1/_2$ 63484.3,	$J=3^1/_2$ 63485.0,	$J=4^1/_2$ 63484.0,	$J=5^1/_2$ 63484.2,
		$J=4^1/_2$	$J=1^1/_2$	$\nu(P_{21})_{cal.}$	$\nu(Q_{11})_{cal.}$		$J=9^1/_2$	63472.9
71.9	3d	63470.0	71.6				$J=10^1/_2$	68.2
			70.3	$J=2^1/_2$			$J=11^1/_2$	62.5
67.4		66.6	68.1	63467.3				
		$J=6^1/_2$		$P=8^1/_2$				
62.5	2	62.4		62.7				
		$J=7^1/_2$	$J=7^1/_2$					
57.0	2	57.5	56.3	57.5				
51.7	2	51.8	50.7	51.5				
44.4	3	45.2	44.2	44.8				
		$J=10^1/_2$	$J=10^1/_2$		$J=7^1/_2$			
36.8	3	37.9	36.9	37.4	63436.0			
29.5	4	29.7	28.8	29.1	27.9			
20.0	5	20.7	19.9	20.0	18.9			
				$J=10^1/_2$	$J=10^1/_2$			
10.2	5	10.9	10.2	10.1	09.1			
63399.5	5	00.3	63399.7	63399.4	63398.5	$\nu(P_{11})_{cal}$		
			$J=15^1/_2$					
87.9	5	63388.9	88.3	87.9	87.0			
						$J=10^1/_2$		
83.0	0					63383.8		
76.3	5	63376.7	76.0	75.6	74.8			
70.1	0					70.6	$\nu(R_{22})_{cal.}$	
		$J=17^1/_2$					$J=2^1/_2$	63863.0
63.3	6d	63.7	63.1	62.5	61.7		$J=3^1/_2$	63.4
							$J=4^1/_2$	63.3
57.3	1					56.7		
48.1	5		49.2	48.5	47.8		$\nu(Q_{12})_{cal.}$	$\nu(R_{12})_{cal.}$
							$J=3^1/_2$	
42.5	2					41.9	42.3	
				$J=16^1/_2$	$J=16^1/_2$		$J=5^1/_2$	$J=7^1/_2$
33.8	4		34.9	33.8	33.1		33.1	33.8
						$J=14^1/_2$	$J=6^1/_2$	
27.0	4					26.4	27.1	27.3
			$J=20^1/_2$				$J=7^1/_2$	$J=9^1/_2$
19.4	5		19.1				20.0	19.8

3. Rotational Analysis of $(B'-B^2\Pi_r)$ System

In the emission spectrum of flowing NO fourteen bands appearing between 5500 A and 8000 A have been assigned to $(B'-B^2\Pi_r)$ system as a result of vibrational analysis[10]. Among them the bands assigned to (0−0) and (3−4) show their rotational structure fairly well without the possibility of overlapping rotational lines of other bands. Rotational analyses of these 6880 A and 7150 A bands have been tried. The spectrum was photographed by a glass spectrograph composed of three 60° prisms of 6 cm base and a camera lens of 50 cm focal length. Although the dispersion is insufficient (65 A/mm for 7000 A) for normal rotational analysis, by the same method as that described in section 2 rotational constants and band origins were obtained, which justify the result of vibrational assignment. It should be mentioned that there is one point different from section 2. Because the lower state of this system, $B^2\Pi$, belongs to quite an intermediate state between case a and b, the rotational terms cannot be approximated by either equation (2) or (3), but can be expressed only by rigorous Hill-Van Vleck formula (eq. (7) in Appendix). Therefore the wave numbers calculated by the equations

Table 4. $(B'-B)$ system; (0−0) band
$B'=1.321$, $\nu_{0,0}^{(1)}=14548$, $\nu_{0,0}^{(2)}=14516$

J	$\nu_{obs.}$	Int.	$\nu(Q_{21})_{cal.}$	$\nu(R_{11})_{cal.}$
$10^1/_2$	14585	1		14586
$11^1/_2$	92	2		93
$12^1/_2$	99	3	14601	14600
$13^1/_2$	14607	3	08	07
$14^1/_2$	16	3	17	16
$15^1/_2$	24	3	25	24
$16^1/_2$	33	3	34	33
$17^1/_2$	44	3	44	43
$18^1/_2$	54	3	54	53

Heads: Violet shade.

$\nu_{obs.}$	Int.	$\nu_{cal.}$	Reference
14492	1	14492	$J=10^1/_2$ and $11^1/_2$ of P_{12}
14511	3_d	512	$J=4^1/_2$ of P_{22} forms a head, followed by clouded lines of $J=2^1/_2$, $3^1/_2$, $5^1/_2\sim9^1/_2$ of P_{22} and $J=2^1/_2\sim8^1/_2$ of Q_{21}
14530	1	529	$J=6^1/_2$ of P_{11}
43 49	4_d	543	$J=3^1/_2$ and $4^1/_2$ of P_{21} form a head, followed by clouded lines of $J=2^1/_2$, $5^1/_2\sim8^1/_2$ of P_{21} and $J=5^1/_2\sim8^1/_2$ of Q_{11}

(3) have a tendency to shift from the actual values as J increases, and it is impossible to get reasonable numbering of J for any value of B' in order to explain the observed wave numbers of four heads and lines well separated only for fairly high J. As for the rotational term values of $v=0$ level of $B^2\Pi$, the difference between the value calculated by the empirical formula of Jenkins, Barton and Mulliken and that obtained by the formula $F(J)=B_{0,1,\mathrm{eff}}J(J+1)$ with $B_{0,1,\mathrm{eff}}=1.070$ amounts to $7.6\,\mathrm{cm}^{-1}$ for $J=20^1/_2$. The difference obtained in this way has been added as the correction for the values calculated by equations (3). The wave numbers thus obtained using $B'=1.321$, $A'=-2$, $\nu_{0,0}^{(1)}=14548$, $\nu_{0,0}^{(2)}=14516$ agree with the observed ones within the experimental error, which can be recognized in Table 4. $\nu_{0,0}^{(1)}$ and $\nu_{0,0}^{(2)}$ mean the wave numbers between the mid point of rotationless states of $v=0$ levels of $B'^2\Delta_{3/2}$ and $B'^2\Delta_{5/2}$ and the rotationless state of $v=0$ levels of $B^2\Pi_{1/2}$ and $B^2\Pi_{3/2}$ respectively.

With reference to the observed values of $\beta(4-3)$ and $\beta(4-2)$ of Schmid[11] the most reasonable constants to explain the structure of (3—4) band of $(B'-B)$ system are determined to be $B'=1.263$, $A'=-2$, $\nu_{3,4}^{(1)}=13999$ and $\nu_{3,4}^{(2)}=13963$.

Table 5. $(B'-B)$ system; (3—4) band
$B'=1.263$, $\nu_{3,4}^{(1)}=13999$, $\nu_{3,4}^{(2)}=13963$

J	$\nu_{obs.}$	Int.	$\nu(Q_{21})_{cal.}$	$\nu(R_{11})_{cal.}$
$16^1/_2$	14087	3	14086	
$17^1/_2$	96	3	14095	14095
$18^1/_2$	14106	4	14105	14105
$19^1/_2$	16	4	16	15
$20^1/_2$	27	4	27	26
$21^1/_2$	39	4	38	38
$22^1/_2$	51	4	50	50
$23^1/_2$	63	4	63	62
$24^1/_2$	75	3		75
$25^1/_2$	87	4		87

Heads; Violet shade.

$\nu_{obs.}$	Int.	$\nu_{cal.}$	Reference
13943	1	13943	$J=6^1/_2$ and $J=7^1/2$ of P_{12}
13956 64	3_d	56	$J=3^1/_2$ of P_{21} forms a head, followed by clouded lines of $J=2^1/_2$, $4^1/_2\sim8^1/_2$ of P_{21} and $J=2^1/_2\sim8^1/_2$ of Q_{21}
13981	1	81	$J=7^1/_2$ of P_{11}
95 14012	4_d	95	$J=3^1/_2$ of P_{21} forms a head, followed by clouded lines of $J=2^1/_2$, $4^1/_2\sim11^1/_2$ and $J=5^1/_2\sim11^1/_2$ of Q_{11}

The meanings of $\nu_{3,4}^{(1)}$ and $\nu_{3,4}^{(2)}$ are the same as those of $\nu_{0,0}^{(1)}$ and $\nu_{0,0}^{(2)}$ above described, except that the vibrational quantum number v is 3 in the upper state instead of zero and that of lower state is 4 instead of zero. Calculated values are compared with observed ones in table 5.

The difference between $\nu_{0,0}^{(1)}$ and $\nu_{0,0}^{(2)}$ above derived should be equal to the doublet splitting of $v=0$ level of $B^3\Pi$. Actually it agrees well with 32.6 cm^{-1} which is the difference of the height between the origins $v=0$ level of $B^3\Pi_{1/2}$ and $B^3\Pi_{3/2}$ calculated using the constants given in the Appendix. However concerning the doublet splitting of $v=4$ level of $B^3\Pi$ the calculated value, 38.15 cm^{-1}, by the use of the constants mentioned above exceeds the difference between $\nu_{3,4}^{(1)}$ and $\nu_{3,4}^{(2)}$, i.e. 36 cm^{-1}, beyond the experimental error in relative position. It might be supposed that the level of $v=4$ of $B^3\Pi$ cannot be expressed in terms of the constants suitable to the levels of $v=0, 1, 2$ and 3.

4. Discussion

The analyses above mentioned show that the upper state of β'-system is an

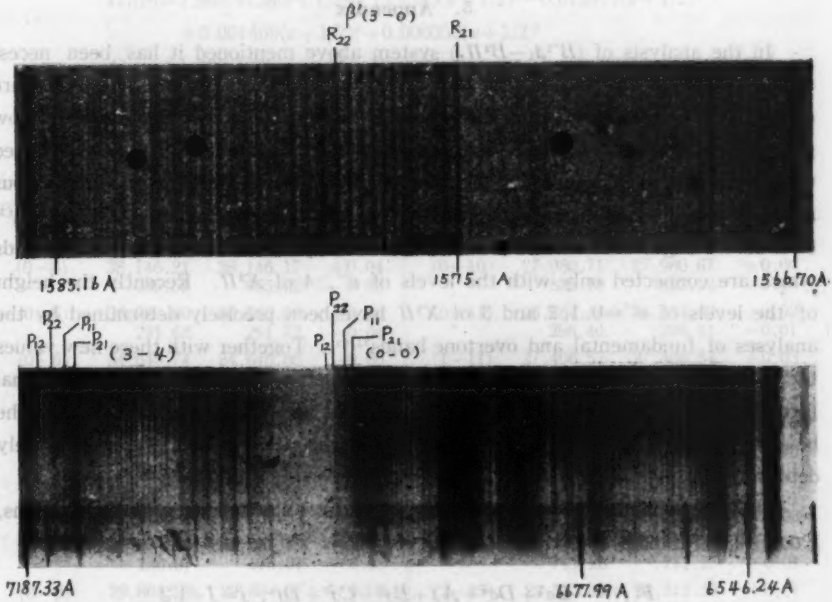

Upper Fig. 1. $\beta'(3-0)$ in the far ultraviolet absorption.
Lower Fig. 2. $(0-0)$ and $(3-4)$ band of $(B'-B)$ system in the near infrared emission.

inverted $^2\Delta$ with coupling constant $A\approx -2$, and the constants obtained by Miescher[1] can be applied to the vibrational levels of $v'=0, 1$ and 3. The values, 49479 cm^{-1} and 49390 cm^{-1}, obtained by subtracting $\nu_{3,4}^{(1)}$ and $\nu_{3,4}^{(2)}$ of (3—4) band of $(B'-B)$ system from the $\nu_{3,0}^{(1)}$ and $\nu_{3,0}^{(2)}$ of $\beta'(3-0)$ band respectively, should be equal to $\nu_{4,0}^{(1)}$ and $\nu_{4,0}^{(2)}$ of $B^2\Pi$. Actually, however, these values are comparatively less than that calculated by the constants obtained in the Appendix, i. e. 49487 cm^{-1} and 49401 cm^{-1}, and the difference between them surely exceeds the experimental error. When $\nu_{4,3}^{(1)}$ and $\nu_{4,3}^{(2)}$ estimated from Schmed's[11] observed values of $\beta(4-3)$ band, and the height[4] of $v=3$ levels of $X^2\Pi$ are adopted the $\nu_{4,0}^{(1)}$ and $\nu_{4,0}^{(2)}$ of $B^2\Pi$ should be 49482 cm^{-1} and 49390 cm^{-1}, which agree fairly well with the observed ones. But from the measured values of $\beta(4-2)$ band of Schmid[11] and the height[4] of $v=2$ levels of $X^2\Pi$, $\nu_{4,0}^{(1)}$ and $\nu_{4,0}^{(2)}$ should be 49486 and 49397 cm^{-1}, which are about 7 cm^{-1} greater than the present estimation. The accurate rotational analysis for bands of β-system relating to the levels of $v'\geq 4$ is desired in this respect and it might also serve to show how the $B^2\Pi$ state is perturbed.

5. Appendix

In the analysis of $(B'^2\Delta_i - B^2\Pi_r)$ system above mentioned it has been necessary to examine the constants of $B^2\Pi$ following the reports on rotational structure of the β-system, because some discrepancies have arisen when the constants now generally used were adopted. As a result of this examination it has been revealed that although the measurement by Jenkins, Barton and Mulliken has marvelous accuracy, their exact empirical formulas have made the values of $\nu_{0,0}^{(1)}$ and $\nu_{0,0}^{(2)}$ of $B^2\Pi$ too high, because the β-bands observed by them are limited to the bands which are connected only with the levels of $v''\geq 4$ of $X^2\Pi$. Recently the height of the levels of $v''=0, 1, 2$ and 3 of $X^2\Pi$ have been precisely determined by the analyses of fundamental and overtone bands[3),4)]. Together with these new values the data reported by Jenkins, Barton and Mulliken were rearranged in the usual formula of recent spectroscopy. The vibrational and rotational constants and the height of $B^2\Pi$ expressed in the notations now generally used were accurately determined.

The rotational terms were represented in the following equation by Jenkins, Barton and Mullken,

$$F(j)=-B\sigma^2+D\sigma^4+Aj+Bj^2+Cj^3+Dj^4;\quad j=J+1/2$$
$$\sigma=1/2 \text{ for } {}^2\Pi_{1/2} \text{ and } \sigma=3/2 \text{ for } {}^2\Pi_{3/2} \qquad (4)$$

and the band origin is considered to be the position of $j=0$ and $\sigma=0$. Therefore

the origin considered to be the height of $J=0$ and $\Omega=0$ in the following formula

$$F(J)=-B\Omega^2+BJ(J+1)-DJ^2(J+1)^2 \qquad (5)$$

is a little lower than the former, but this difference is in the region of experimental error and negligible especially when the ΔG_v values are adopted to estimate vibrational constants. Consequently the observed band origins by Jenkins, Barton and Mullikens themselves are here used.

The vibrational formula of $X^2\Pi$ obtained by the measurement in the infrared[3),4)] explains well the observed values of Jenkins, Barton and Mulliken[2)] to the height of $v=11$ level of $X^2\Pi_{1/2}$ and $v=10$ level of $X^2\Pi_{3/2}$. If the lower state of β-system is assumed to be expressed in these formulas, the values of $\nu_{0,0}^{(1)}$ and $\nu_{0,0}^{(2)}$ should be 45,482.69 cm^{-1} and 45,390.75 cm^{-1} respectively, which are about 3~4 cm^{-1} less than the values now generally used.

As a result of the least square method to determine the constants most suitable to the levels of $X^2\Pi$ from $v=0$ up to $v=16$ the next two equations are obtained.

$$\begin{aligned} G_1(v)&=1{,}903.9736(v+1/2)-13.9355(v+1/2)^2-0.013177(v+1/2)^3 \\ &\quad +0.001409(v+1/2)^4-0.000053(v+1/2)^5 \\ G_2(v)&=1{,}903.4005(v+1/2)-13.8292(v+1/2)^2-0.028299(v+1/2)^3 \\ &\quad +0.002283(v+1/2)^4-0.000071(v+1/2)^5 \end{aligned} \qquad (6)$$

Table 6.
Frequencies of band origins

Band	$\nu_{obs.}$	$\nu_{cal.}$	o−c	Band	$\nu_{obs.}$	$\nu_{cal.}$	o−c
(0−4)	38,146.21	38,146.17	+0.04	(0−10)	27,980.71	27,980.67	+0.04
	055.59	055.62	−0.03		892.18	892.12	+0.04
(0−5)	36,382.00	36,382.00	±0.00	(0−11)	26,384.44	26,384.42	+0.02
	291.68	291.72	−0.04		296.40	296.41	−0.01
(0−6)	34,645.74	34,645.80	−0.06	(1−11)	27,406.57	27,406.54	+0.03
	555.77	555.82	−0.05		319.95	319.93	+0.02
(1−6)	35,667.69	35,667.92	−0.23	(0−12)	24,816.31	24,816.32	−0.01
	579.24	579.34	−0.10		728.69	728.77	−0.08
(0−7)	32,937.54	32,937.56	−0.02	(1−13)	24,298.63	24,298.63	±0.00
	847.91	847.91	±0.00		212.95	212.96	−0.01
(0−8)	31,257.27	31,257.28	−0.01	(2−13)	25,306.41	25,306.42	−0.01
	168.04	168.00	+0.04		222.10	222.13	−0.03
(3−8)	34,281.14	34,281.15	−0.01	(2−14)	23,795.06	23,795.06	±0.00
	196.07	196.01	−0.05		711.28	711.27	+0.01
(0−9)	29,604.99	29,604.97	+0.02	(2−15)	22,312.40	22,312.39	+0.01
	516.10	516.09	+0.01		229.13	229.14	−0.01
(2−9)	31,634.78	31,634.88	−0.10	(3−16)	21,852.65	21,852.65	±0.00
	548.80	548.78	+0.02		771.36	771.36	±0.00

$\nu_{0,0}^{(1)}$ and $\nu_{0,0}^{(2)}$ should be 45,482.64 cm^{-1} and 45,390.87 cm^{-1} respectively, according to the observed values of the β-system and the height of each vibrational level of $X^2\Pi$ calculated by the above formulas.

The vibrational formulas of $B^2\Pi$ are estimated as follows:

$$G_1(v)=1{,}036.929(v+1/2)-7.5399(v+1/2)^2+0.0833(v+1/2)^3$$

$$G_2(v)=1{,}038.349(v+1/2)-7.5499(v+1/2)^2+0.0833(v+1/2)^3$$

When these new constants are adopted to calculate band origins of the β-system the observed and calculated values are in agreement exactly within the experimental error, which can be recognized in Table 6.

According to the constants now derived the values of T_e of $B^2\Pi_r$ cited in the table of Herzberg[14] are to be 45,914.55 cm^{-1} and 45,492.91 cm^{-1}, which have decreased about 3~4 cm^{-1}. It should be noted here that the constants of $B^2\Pi_r$ have been derived from the levels of $v' \leq 3$ only, so have the tendency to show higher values for levels with $v' \geq 4$ than can be estimated from the observed heads of β-bands in absorption[15].

Although equation (4) is quite convenient to estimate the actual height of rotational terms the rotational constant B_v is defined by the following equations for such a state as $B^2\Pi$, that is precisely an intermediate state between case a and b;

$$F_1(J)=B_v[(J+1/2)^2-\Lambda^2-1/2\sqrt{4(J+1/2)^2+Y(Y-4)\Lambda^2}]-D_vJ^4$$

$$F_2(J)=B_v[(J+1/2)^2-\Lambda^2+1/2\sqrt{4(J+1/2)^2+Y(Y-4)\Lambda^2}]-D_v(J+1)^4 \quad (7)$$

therefore

$$\Delta_2F_1+\Delta_2F_2=4(J+1/2)(2B_v-7D_v)-16D_v(J+1/2)^3$$

Using the mean values of Δ_2F for various vibrational states of Jenkins, Barton and Mulliken, the values of $(\Delta_2F_1+\Delta_2F_2)/(J+1/2)$ are plotted versus $(J+1/2)^2$, which forms almost a straight line. The value of D_v was first determined from the slope of this line, from whose intercept on the ordinate axis B_v can be determined. The value B_v thus obtained is likely to be 0.0002~0.001 cm^{-1} greater than that which can be estimated by the tangent of $(\Delta_2F_1+\Delta_2F_2)$ versus $(J+1/2)$ curve at $J=0$. B_v in Table 7 is the average of the former and the latter. Both B_v and D_v change linearly with v and the values of B_e, α_e, D_e and β_e are easily determined, and are listed in Table 7.

14) G. Herzberg: Molecular Spectra and Molecular Structure I (1950) 558.
15) Y. Tanaka: Sci. Pap. Inst. Physic. Chem. Res. (Tokyo) **43** (1948) 28.

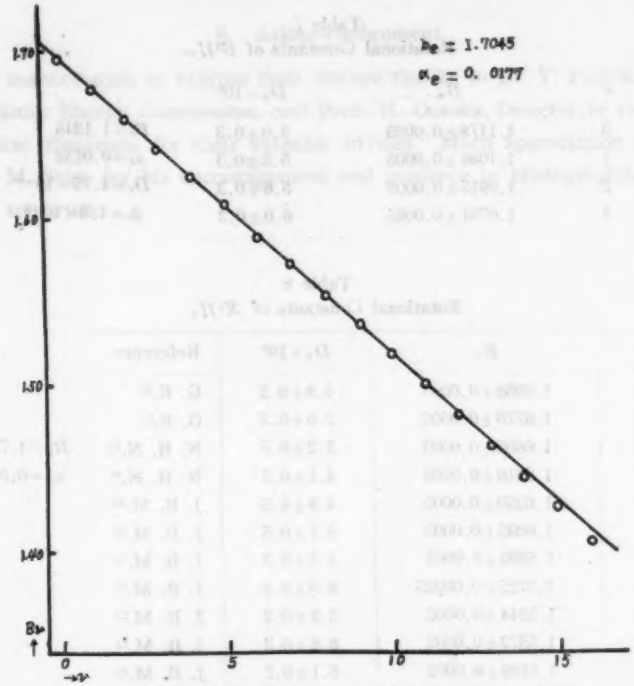

Fig. 3. Graphical determination of B_e and α_e of $X^3\Pi$

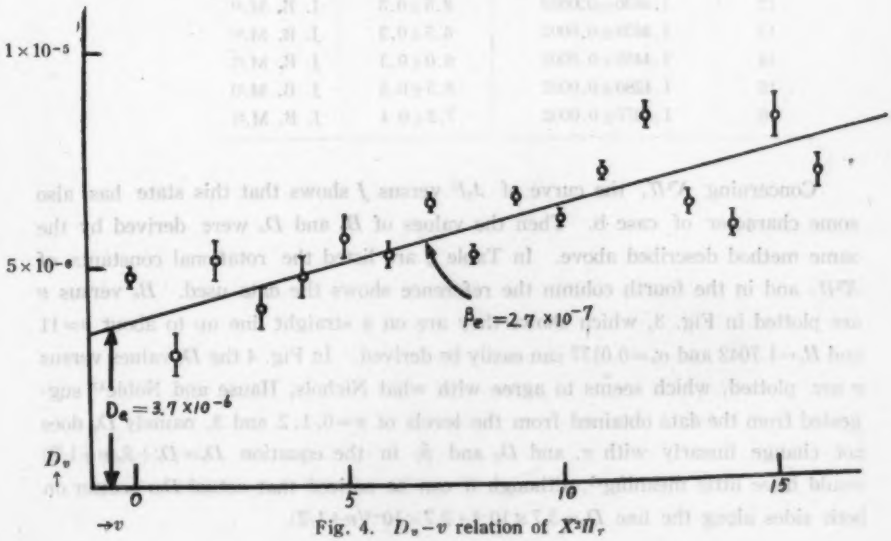

Fig. 4. $D_v - v$ relation of $X^3\Pi_r$

Table 7.
Rotational Constants of $B^3\Pi_r$.

v	B_v	$D_v\times10^6$	
0	1.1178±0.0005	5.0±0.3	$B_e=1.1245$
1	1.1046±0.0005	5.3±0.3	$\alpha_e=0.0132$
2	1.0915±0.0005	5.6±0.3	$D_e=4.75\times10^{-6}$
3	1.0791±0.0005	6.0±0.3	$\beta_e=1.3\times10^{-6}$

Table 8
Rotational Constants of $X^3\Pi_r$

v	B_v	$D_v\times10^6$	Reference	
0	1.6958±0.0005	4.8±0.2	G. E.[3]	
1	1.6770±0.0005	3.0±0.5	G. E.[3]	
2	1.6605±0.0005	5.2±0.5	N. H. N.[4]	$B_e=1.7045$
3	1.6410±0.0005	4.1±0.5	N. H. N.[4]	$\alpha_e=0.0177$
4	1.6250±0.0005	4.8±0.5	J. B. M.[2]	
5	1.6095±0.0003	5.7±0.5	J. B. M.[2]	
6	1.5893±0.0003	4.3±0.3	J. B. M.[2]	
7	1.5725±0.00025	6.5±0.2	J. B. M.[2]	
8	1.5544±0.0002	5.3±0.2	J. B. M.[2]	
9	1.5372±0.0002	6.6±0.2	J. B. M.[2]	
10	1.5189±0.0002	6.1±0.2	J. B. M.[2]	
11	1.5007±0.0002	7.2±0.2	J. B. M.[2]	
12	1.4830±0.0002	8.5±0.3	J. B. M.[2]	
13	1.4638±0.0002	6.5±0.3	J. B. M.[2]	
14	1.4450±0.0002	6.0±0.3	J. B. M.[2]	
15	1.4280±0.0002	8.5±0.5	J. B. M.[2]	
16	1.4077±0.0002	7.2±0.4	J. B. M.[2]	

Concerning $X^3\Pi$, the curve ρf Δ_2F versus J shows that this state has also some character of case b. Then the values of B_v and D_v were derived by the same method described above. In Table 8 are listed the rotational constants of $X^3\Pi_r$ and in the fourth column the reference shows the data used. B_v versus v are plotted in Fig. 3, which shows they are on a straight line up to about $v=11$ and $B_e=1.7042$ and $\alpha_e=0.0177$ can easily be derived. In Fig. 4 the D_v values versus v are plotted, which seems to agree with what Nichols, Hause and Noble[4] suggested from the data obtained from the levels of $v=0, 1, 2$ and 3, namely D_v does not change linearly with v, and D_e and β_e in the equation $D_v=D_e+\beta_e(v+1/2)$ would have little meaning[4], although it can be noticed that actual D_vs scatter on both sides along the line $D_v=3.7\times10^{-6}+2.7\times10^{-7}(v+1/2)$.

6. Acknowledgement

The authors wish to express their sincere thanks to Dr. Y. Fujioka, Member of the Atomic Energy Commission, and Prof. H. Ootuka, Director of the Institute for Optical Research, for their valuable advices. Much appreciation is also due to Prof. M. Seya for his encouragement and guidance in photographing the absorption spectrum.